UNIVERSITÀ DEGLI STUDI DI NAPOLI FEDERICO II

DIPARTIMENTO DI AGRARIA

TESI DI DOTTORATO
DOTTORATO IN VALORIZZAZIONE E GESTIONE DELLE RISORSE
AGRO-FORESTALI

CICLO XXV
(A.A. 2012/2013)

SELF-ORGANIZATION IN THE DEVELOPMENT OF

PLANT SPATIAL PATTERNS

COORDINATORE:
PROF. GUIDO D'URSO

TUTOR:
DOTT. FRANCESCO GIANNINO

CO-TUTOR:
PROF. STEFANO MAZZOLENI

DOTTORANDO:
FABRIZIO CARTENÌ

CONTENTS

_____

ABSTRACT

_____

The study of self-organization is a relatively new field that received great attention in the last decades related to the study of complex systems. In particular, self-organizing properties of some systems are particularly important in the development of spatial patterns, and their analysis could lead to interesting insights into their functioning. Self-organization is a process in which pattern at the global level of a system emerges solely from the interactions among the lower-level components of the system and the best tool to study such interactions is the use of mathematical models to simulate the emergent behaviour of the system.

This thesis addresses two specific problems related to pattern formation in plants at different scales. The first topic is the emergence of vegetation patterns at landscape level. Different putative mechanisms have been proposed as drivers of vegetation pattern formation in different environments. The most studied mechanism is related to short range positive feedbacks and long range negative feedbacks between plants and the available water. Such explanation provides important insights on the dynamics of arid and semiarid environments where water is a limiting factor, but fails to explain the emergence of similar patterns in humid environments. For this reason we formulated a mathematical model to test the effects of the release of autotoxic compounds during litter decomposition, i.e. plant-soil negative feedback, on the emergence of vegetation patterns, in particular the formation of ring structures by clonal plants. Model simulations show that the formation of rings can be explained by autotoxicity and that resource scarcity is not a necessary condition. Moreover, we further developed the model to consider both water and toxic compounds influences on plant biomass growth in order to assess the relative importance of the two mechanisms. Numerical simulations show that water/biomass feedbacks lead to stable spatial patterns, while autotoxicity has a destabilizing effect on the system, leading to unstable patterns that continuously evolve in time.

The second topic is the differentiation of primary vascular patterns at cellular/tissue level. Most of the attention has focused on the genetic regulation and the hormonal control of specific aspects of the development of vascular tissues. In this study, we formulated a model defining a set of logical and functional rules to simulate the differentiation of procambium, phloem and xylem and their emerging spatial patterns, starting from an homogeneous group of undifferentiated cells. Specific attention has been given to the factors responsible for the intra- and inter-specific variability of the arrangements observed in plants. Simulation results show that the model is capable of reproducing most vascular patterns observed in plants, from primitive and simple structures constituted of a single strand of vascular bundles (protostele), to more complex and evolved ones, with separated vascular bundles arranged in an ordered pattern within the plant section (e.g. eustele). Presented results demonstrate, as a proof of concept, that a common genetic-molecular machinery can be at the base of different spatial patterns of plant vascular tissues.

1

INTRODUCTION

The study of self-organization is a relatively new field, but it has already received great attention producing a large body of literature on different topics. Generally, self-organization is defined as a process where a system evolves into an organized form in absence of external pressures. An interesting definition, related to pattern formation in biological systems, is provided by Camazine *et al.* (2001):

"Self-organization is a process in which pattern at the global level of a system emerges solely from numerous interactions among the lower-level components of the system. Moreover, the rules specifying interactions among the system's components are executed using only local information, without reference to the global pattern."

A more general definition is provided by Haken (2006):

"A system is self-organizing if it acquires a spatial, temporal, or functional structure without specific interference from the outside. By 'specific' we mean that the structure or functioning is not impressed on the system but that the system is acted upon from the outside in a non-specific fashion. For instance, the fluid which forms hexagons is heated from below in an entirely uniform fashion and it acquires its specific structure by self-organization."

Self-organization occurs in a huge variety of physical, chemical, biological and social systems. Common examples are crystallization, convection patterns of heated fluids, formation of sand dunes, swarm behaviour of animals, spontaneous folding of proteins, formation of patterns in animal coats and the way neural networks learn to recognize complex patterns.

The role of self organization in vegetation pattern formation

The origin of regular spatial patterns in ecological systems has long fascinated researchers. The activator–inhibitor principle, originally proposed by Turing (1952), provided a potential mechanistic explanation for the emergence of regular patterns in biology (Meinhardt 1982; Murray 2002; Kondo and Miura 2010) and chemistry (Castets *et al.* 1990; Ouyang and Swinney 1991). More recently, this principle has been applied to different ecological systems such as arid and semiarid bushlands (Klausmeier 1999; von Hardenberg *et al.* 2001; Rietkerk *et al.* 2002; Ravi *et al.* 2008), mussel beds (van de Koppel *et al.* 2005), and boreal peatlands (Eppinga *et al.* 2008, 2009). The abovementioned studies are essentially based on the principle of scale-dependent feedbacks (Rietkerk and van de Koppel 2008). Ecosystems are essentially composed of organisms and the environment, which interact with each other in different ways. Such interactions can be positive if, for instance, the organisms help each other by modifying the environment through facilitation, or can be negative since they generally compete for a common resource. The occurrence of such feedbacks at different spatial scales (i.e. scale-dependent) can lead to symmetry breaking and the emergence of heterogeneous spatial patterns even without underlying environmental heterogeneity. Considering the example of vegetation dynamics in arid ecosystems, the main limiting

resource is, obviously, water. In this context, plants have a local positive effect on each other through the disruption of the soil-crust that inhibits water infiltration in soil, thus facilitating each other over short distances. On the other hand, plants also compete with each other since water is a limiting factor, creating a long range negative feedback. The co-occurrence of these processes is thought to be responsible for the formation of spatial patterns such as the *tiger bush* (stripes), the *leopard bush* (spots), labyrinths and gaps in such environments. Other examples of scale dependent dynamics are reviewed in (Rietkerk and van de Koppel 2008) although they all relate pattern emergence to the scarcity of a specific resource. Other peculiar vegetation patterns observed in different environments are regularly shaped rings formed by clonal plants. Also called fairy rings, central die-back and monk's tonsure-like gaps, they are observed both in water and nutrient deprived environments like deserts and peatlands as well as in mountain and alluvional grasslands and in salt marshes where water is not a limiting factor.

Recently, a new hypothesis has been proposed that could provide an explanation for the emergence of spatial patterns without limiting resources. Species-specific plant-soil Negative Feedback (NF) has been defined as the rise of negative conditions for plant vegetative and reproductive performances induced in the soil by the plants themselves and has been described for many plant species (Mazzoleni *et al.* 2007; Kulmatiski *et al.* 2008). Such effect can both be intra- and inter- specific (Oremus and Otten 1981; van der Putten *et al.* 1993; Bever 1994; Singh *et al.* 1999; Packer and Clay 2000; Klironomos 2002; Kardol *et al.* 2007; Mazzoleni *et al.* 2007) and has been related to different mechanisms such as depletion of soil nutrients (Ehrenfeld *et al.* 2005), build up of soil-borne pathogens (van der Putten *et al.* 1993; Packer and Clay 2000), shifts of soil microbial communities (Bever 1994; Klironomos 2002; Kardol *et al.* 2007), and phytotoxicity of decomposing plant litter (Webb *et al.* 1967; Singh *et al.* 1999; Armstrong and Armstrong 2001). Evidence for autotoxicity is abundant in agriculture (reviewed in Singh *et al.* 1999) and also present in some ecological studies (Webb *et al.* 1967; Armstrong and Armstrong 2001; Perry *et al.* 2005; Bonanomi, Rietkerk, *et al.* 2007). Plant-soil negative feedback has been also considered as the driver of plant species coexistence (Bonanomi, Giannino, *et al.* 2005) and tree species diversity along a latitudinal gradient in a recent modelling work (Mazzoleni *et al.* 2010).

Regarding the occurrence of rings of clonal plants and other spatially heterogeneous vegetation patterns in ecosystems where resources may or may not be limiting factors, I specifically address the following research questions (RQ):

RQ1. Can plant-soil negative feedback and, specifically, autotoxicity explain the formation of ring patterns in conditions where water is not a limiting factor?

RQ2. What are the interactions between biomass-water feedbacks and the negative feedback between plant biomass and toxic compounds released during litter decomposition?

The role of self organization in the development of plants

The control of development in higher organisms is one of the most fascinating problems in biology. How development proceeds must be somehow genetically determined, but genetic and biochemical investigations alone are not sufficient to lead to a full understanding of the problem because of the difficulty to infer cause/effect relationships between different events. Recently, process-based mathematical models have provided new insights in this context.

Most of the attention has focused on the hormonal control, auxin in particular, and the genetic regulation of development. Plant hormones regulate many aspects of growth (Wolters and Jürgens 2009). Auxin seems to have a central role and has been the centre of many studies. Critical to the auxin dynamics is its polar transport which is mediated by membrane-bound influx and efflux carriers, i.e. AUX and PIN family proteins. In roots such carriers are

expressed in static patterns that were used to predict auxin distribution in the organ. Grieneisen *et al*. (2007) implemented fixed PIN patterns in a two-dimensional model showing that this was sufficient to create an experimentally verified stable auxin maximum at the root apex, also predicting several perturbations. Recently, Muraro *et al*. (2013) developed a simulation model incorporating auxin and cytokinin signalling networks and transport dynamics to study their involvement in xylem and procambium specification in root radial sections of *Arabidopsis*. In other contexts (e.g. leaf venation), auxin patterning shows a more dynamic localization of carriers. The first model was formulated by Sachs (1969) proposing the so called "canalization hypothesis", i.e., auxin export through a cell wall promotes further transport in the same direction, thus creating canals of preferential flow as a self-organization property of the system. Based on this hypothesis, many molecular models were formulated (e.g. Mitchison 1980; Feugier *et al*. 2005; Bayer *et al*. 2009).

Genetic regulation has a fundamental role in the study of other developmental events. Cellular differentiation leading to trichome formation appears at the epidermis in young leaves and in roots, and the underlying genetic networks seem to be similar (Pesch and Hülskamp 2004; Benítez *et al*. 2007). The molecular mechanisms represent a classical reaction-diffusion model where proteins activate and repress each other and also transport between cells is present. Digiuni *et al*. (2008) used a deterministic differential equation model to support their new data on protein transport and could discriminate between different hypotheses for the formation of a competing inactivated complex in the leaf. With a different approach, Savage *et al*. (2008) used a stochastic Boolean model to show that the often used self-activation of one of the activators could not explain all mutant data available for the root. Another example is the spatial and temporal organization of the shoot apical meristem (SAM) which is responsible for the formation of all above-ground organs. Many proteins have been discovered to be important in SAM regulation and, of particular interest, the feedback loop between CLAVATA (CLV) and WUSCHEL (WUS). Jönsson *et al*. (2003, 2005) used a multicellular model to investigate different aspects of the CLAVATA/WUSCHEL feedback. They provided a hypothesis for how the asymmetric localization of a CLV3 region from the activating WUS region could appear (Jönsson *et al*. 2003), and demonstrated how a spatially restricted activation of WUS via a reaction-diffusion dynamics was sufficient to explain the spontaneous organization and perturbed reorganization of the WUS domain (Jönsson *et al*. 2005). Fujita *et al*. (2011) developed a mathematical model of the SAM, including the WUS/CLV dynamics, the spatial restriction of such dynamics and cell division. The model was capable of reproducing the different SAM patterns observed in plants as well as aberrant patterns generated in *wus* and *clv* mutants.

Although the abovementioned simulation models have tackled many specific issues related to plant development, a complete understanding of the dynamic behaviour of such processes is still to be achieved. In particular, still no effort has been done to put together all the steps leading to the specification of provascular tissues and primary phloem and xylem. Related to the genetic and molecular interactions involved in the differentiation of vascular tissues in plants and also the diversity of patterns observed in nature, I specifically address the following RQ:

RQ3. Is it possible that a single genetic and molecular machinery can account for all the primary vascular patterns of plants? What are the possible mechanisms and processes responsible for intra- and inter-specific variation?

Outline of the thesis

In Chapter 2, we develop a reaction-diffusion mathematical model to address the effects of plant-soil negative feedback on the emergence of ring spatial patterns in ecosystems where water is not a limiting factor (RQ1). The model describes the spatial and temporal dynamics of a clonal plant biomass and autotoxic compounds released in soil as a result of litter decomposition.

In Chapter 3, we further investigate the effects of plant-soil negative feedback on pattern formation, also including the interactions with the plant-water positive and negative feedbacks. To address this issue (RQ2) we devised a mathematical model starting from published works that studied the interactions between plant biomass and water, also including the autoinhibitory effects discussed in Chapter 2.

In Chapter 4, we apply the same reaction-diffusion modelling approach to study a different problem: the differentiation of plant vascular tissues. Inspired by the work of Meinhardt (1982) on biological pattern formation, we introduce a new modular mathematical model to address the differentiation of phloem and xylem with a specific focus on the factors responsible for the emergence of the different primary vascular arrangements observed in nature (RQ3).

In Chapter 5, I bring all the results together and conclude highlighting the questions raised by this work that will be the subject of future investigations.

2

NEGATIVE PLANT SOIL FEEDBACK EXPLAINING RING FORMATION IN CLONAL PLANTS

_____

Fabrizio Cartenì, Addolorata Marasco, Giuliano Bonanomi, Stefano Mazzoleni, Max Rietkerk, Francesco Giannino.

Abstract

Ring shaped patches of clonal plants have been reported in different environments, but the mechanisms underlying such pattern formation are still poorly explained. Water depletion in the inner tussocks zone has been proposed as a possible cause, although ring patterns have been also observed in ecosystems without limiting water conditions. In this work, a spatially explicit model is presented in order to investigate the role of negative plant-soil feedback as an additional explanation for ring formation. The model describes the dynamics of the plant biomass in the presence of toxicity produced by the decomposition of accumulated litter in the soil. Our model qualitatively reproduces the emergence of ring patterns of a single clonal plant species during colonization of a bare substrate. The model admits two homogeneous stationary solutions representing bare soil and uniform vegetation cover which depend only on the ratio between the biomass death and growth rates. Moreover, differently from other plant spatial patterns models, but in agreement with real field observations of vegetation dynamics, we demonstrated that the pattern dynamics always lead to spatially homogeneous vegetation covers without creation of stable Turing patterns. Analytical results show that ring formation is a function of two main components, the plant specific susceptibility to toxic compounds released in the soil by the accumulated litter and the decay rate of these same compounds, depending on environmental conditions. These components act at the same time and their respective intensities can give rise to the different ring structures observed in nature, ranging from slight reductions of biomass in patch centres, to the appearance of marked rings with bare inner zones, as well as the occurrence of ephemeral waves of plant cover. Our results highlight the potential role of plant-soil negative feedback depending on decomposition processes for the development of transient vegetation patterns.

1. Introduction

The occurrence of regularly shaped circles or rings of clonal plants has been documented since long time (Watt 1947; Curtis and Cottam 1950; Cosby 1960). Clonal plant establishment starts with spots of highly aggregated ramets. However, as new ramets develop centrifugally, their density in the patch interior decreases, with senescence of older shoots and appearance of a ring belt (see Fig. 2.1).

Figure 2.1. Examples of ring forming plants in different ecosystems: (a-b) *Sesleria appennina* in alpine conditions; (c-d) *Brachypodium rupestre* in mountain grassland; (e-f) *Ampelodesmos mauritanicus* in semiarid Mediterranean grassland; (g-h) *Scirpus holoscoenus* in alluvial grassland. The last picture (h) refers to the same individual reported in (g) after its excavation to show the tussock ring shape. All photographs by G. Bonanomi.

Such pattern has been also reported as fairy rings (Hitchcock 1935), rings (Watt 1947), central die-back (Adachi *et al*. 1996), monk's tonsure-like gaps (Lewis *et al*. 2001), and often observed in resources deprived environments including water and nutrient limited ecosystems such as deserts (Danin 1996; Sheffer *et al*. 2007), peatland (Lanta *et al*. 2008), and primary succession over bare substrate (Adachi *et al*. 1996). The mechanisms underlying the formation of plant rings are still poorly known. Water depletion in the inner zone of the ring has been proposed as a possible explanation of central die-back and, consequently, of ring

patterns formation (Ravi *et al*. 2008; Sheffer *et al*. 2011). However, clonal ring perennial plants have been also observed in ecosystems without water limiting conditions. Examples include the grasses *Brachypodium rupestre* (Bonanomi and Allegrezza 2004) (see Fig. 2.1), *Bromus inermis* in mountain grasslands (Otfinowski 2008), the sedge *Scirpus holoshoenus* in alluvial grassland (Bonanomi, Rietkerk, *et al*. 2005) (Fig. 2.1), and several species of *Spartina* in salt marshes (Caldwell 1957; Castellanos *et al*. 1994). It is quite obvious that in these cases the water limitation hypothesis cannot be considered as an exhaustive explanation.

Alternatively, central die-back could be induced by the build-up of negative plant-soil feedback in the inner clonal zone (Curtis and Cottam 1950; Bonanomi, Rietkerk, *et al*. 2005). Negative plant-soil feedback is defined as the rise of negative conditions for plant vegetative and reproductive performances induced in the soil by the plants themselves (Mazzoleni *et al*. 2007). Recognized mechanisms producing negative plant-soil feedback are: the soil nutrient depletion (Ehrenfeld *et al*. 2005), the build-up of soil-borne pathogen populations (Packer and Clay 2000), the changing composition of soil microbial communities (Klironomos 2002), and the release of autotoxic compounds during organic matter decomposition (Singh *et al*. 1999). Curtis and Cottam (Curtis and Cottam 1950) provided the first evidences supporting the negative feedback hypothesis based on litter autotoxicity, by studying the prairie sunflower *Heliantus rigidus*. This perennial forb in the field showed clones with central die-back. The removal of dead roots and rhizomes, which in laboratory had autotoxic effects, improved *H. rigidus* growth, while no positive effect was found after application of mineral nutrients. Moreover, the authors replaced, in open field, the soil present inside the ring with soil collected in the external grassland not previously affected by the same species. This greatly enhanced the biomass recovery of *H. rigidus* in the die-back zone. Following experimental studies provided evidence that herbaceous plant with phalanx growth strategy accumulate large amount of leaves, rhizome and root litter in the die-back zone of the clones (e.g. Watt 1947; Curtis and Cottam 1950; Falinska 1995; Danin 1996; Lanta *et al*. 2004; Bonanomi, Rietkerk, *et al*. 2005), that negatively affect conspecific regeneration. As a consequence, negative feedback escape strategies depend on life form and propagation patterns. For instance, trees and shrubs can avoid the "home" soil (sensu Bever 1994) via seed dispersal, thus producing a Janzen-Connell distribution of seedling emergence (Packer and Clay 2000; Bonanomi, Antignani, *et al*. 2007), while perennial clonal plants with "phalanx" growth strategy (Doust 1981) can move away by vegetative growth thus forming rings (Olff et al. 2000; van der Putten 2003; Bonanomi, Rietkerk, et al. 2005).

Recently, a substantial modelling effort has been done to investigate the mechanisms underlying the formation of several types of vegetation patterns in water-limited ecosystems (Rietkerk *et al*. 2002; Gilad *et al*. 2007; Meron *et al*. 2007; Barbier *et al*. 2008). Despite of a significant body of empirical studies on plant forming rings, only a few models have been developed to explain the appearance of such patterns in clonal plants. Available models addressed the possible role of water limitation on the formation of plant rings in semiarid environments (Sheffer *et al*. 2007; von Hardenberg *et al*. 2010). Here, we investigated the possibility that negative plant-soil feedback may be considered an additional explanation for ring formation in clonal plants with "phalanx" propagation strategy. The mathematical models proposed in (Bever *et al*. 1997; Bonanomi, Giannino, *et al*. 2005) demonstrated, by means of non-spatial simulations, how intra-specific negative feedback can allow species coexistence, by creating unsuitable conditions for conspecifics, and suitable conditions for other species. However, to our knowledge, no studies explored the potential effects of negative plant-soil feedback resulting from toxic compounds during litter decomposition for the formation of vegetation patterns.

In this paper, first we introduce a spatially explicit model for biomass dynamics of one clonal plant, derived by the model described in Mazzoleni *et al*. (2010), to investigate the role of intra-specific plant-soil negative feedback conceived as the product of litter toxicity

10

(Bonanomi *et al*. 2006) and autotoxicity (Blok and Bollen 1993; Singh *et al*. 1999; Mazzoleni *et al*. 2007). Then, we develop a qualitative and quantitative analysis of the model, with special attention to the main mechanisms underlying pattern formation. This section contains the mathematical study of the model, including stability analysis of the homogeneous steady-state values, linear stability analysis to spatially heterogeneous perturbations and an estimate of the "invasion velocity" of the plant biomass. Finally, we discuss the implications of the presented mechanism in the framework of water-limitation induced pattern formation.

2. The mathematical model

Based on the work of Mazzoleni *et al*. (2010), we introduce a model for biomass dynamics of one clonal plant with phalanx growth strategy and for the rising tussock spatial patterns induced by negative plant-soil feedback. Beginning from an initial small tussock of tillers, roots and rhizomes surrounded by bare soil (Fig. 2.2, panel A), the plant starts to propagate colonizing the soil around it in any direction. As the propagation proceeds, dead tillers, roots and rhizomes start to accumulate in the central area of the tussock, where the plant is older. During decomposition of these residues, litter degradation and microbial activity produce phytotoxic materials (Bonanomi *et al*. 2006) with a direct harmful effect on plants. Also, plant resistance to pathogens attack can be reduced by the phytotoxic conditions (Patrick and Toussoun 1965; Bonanomi, Antignani, *et al*. 2007). Moreover, decaying organic matter provides the growth substrate for saprophytic pathogens, thus enhancing their pathogenicity (Hoitink and Boehm 1999; Blomqvist *et al*. 2000; Bonanomi *et al*. 2010; Bonanomi, Antignani, *et al*. 2011). Recent work on phytotoxicity dynamics is clearly showing such trends of toxicity relation with litter decomposition processes (Bonanomi, Incerti, *et al*. 2011). As previously stated, the raise of negative conditions is concentrated in the older (central) part of the tussock thus reducing the growth performance of the plant (Fig. 2.2, panel B). In real conditions, toxicity persistence is linked to litter-decaying rate and, consequently, to related environmental conditions such as temperature and water availability. For simplicity, in this model, toxicity is reduced in time by a constant decay/removal process of toxic compounds (Bonanomi *et al*. 2006; Bonanomi, Incerti, *et al*. 2011).
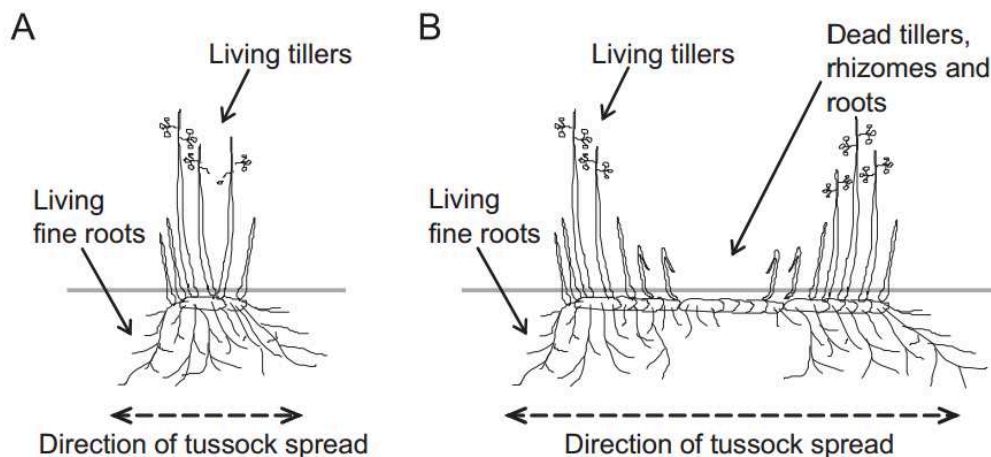
Figure 2.2. Schematic representation of a clonal plant structure during vegetative propagation with phalanx strategy. Starting from an initial small tussock of tillers, roots and rhizomes (A) the plant begins to propagate, colonizing the surrounding soil in every direction. As the propagation proceeds, dead tillers, roots and rhizomes start to accumulate in the central tussock area, where the plant is older. The accumulation of dead biomass and its consequent decomposition, releasing autotoxic compounds, reduces the plant growth performance (B).

2.1. Model description

The model consists of a system of two nonlinear partial differential equations describing the dynamics of two state variables: plant biomass B (kg cm^{-2}) and toxic compounds T (kg cm^{-2}). Plant biomass changes as a function of plant growth, mortality and vegetative propagation. In the mathematical modelling, plant root and shoot were not considered separately because functional root system and living shoot are in close proximity in clonal plants with phalanx growth strategy (Bonanomi, Rietkerk, *et al.* 2005). Plants grow logistically with growth rate parameter g (month^{-1}) and carrying capacity B_{max} (kg cm^{-2}). Plant mortality is due to a constant loss rate d (month^{-1}) and an extra loss induced by the negative plant-soil feedback function of T concentration by means of a parameter s (cm^2 kg^{-1} month^{-1}). Plant vegetative propagation is approximated by a diffusion term of coefficient D (cm^2 month^{-1}). Toxic compounds are produced by a fraction of the dead biomass c (dimensionless) and is reduced by litter removal or decay process simply summarized by a parameter k (month^{-1}) which is the removal/decay rate of T. For simplicity no diffusion of T is considered by the model.

The model parameters descriptions are summarized in Table 2.1. In all simulations the parameter values are chosen according to either Mazzoleni *et al.* (2010) or set to order-of-magnitude realistic values.

Owing to the above description, the model equations are

$$\begin{cases} \dfrac{\partial B}{\partial t} = gB\left(1 - \dfrac{B}{B_{max}}\right) - B(d + sT) + D\Delta B, \\[2mm] \dfrac{\partial T}{\partial t} = cB(d + sT) - kT. \end{cases} \tag{1}$$

In this paper, we studied the model only for positive values of the parameters g, d, s, D, c, k, since for $s = 0$ the nonlinear partial differential equations (1) are decoupled, and for $k = 0$ the model refers to a system in which there is no toxicity decomposition.

In order to minimize the number of parameters involved in the model it is extremely useful to write the system (1) in nondimensional form. Introducing the following dimensionless variables

$$\widetilde{B} = \frac{B}{B_{max}}, \quad \widetilde{T} = \frac{k}{cdB_{max}}T, \quad \widetilde{x} = x\left(\frac{g}{D}\right)^{1/2}, \quad \widetilde{y} = y\left(\frac{g}{D}\right)^{1/2}, \quad \widetilde{t} = gt,$$

then system (1) becomes

$$\begin{cases} \dfrac{\partial B}{\partial t} = B(1 - B) - \alpha B(1 + \beta T) + \Delta B, \\[2mm] \dfrac{\partial T}{\partial t} = \gamma B(1 + \beta T) - \gamma T, \end{cases} \tag{2}$$

where $\alpha = d/g$, $\beta = (csB_{max})/k$, $\gamma = k/g$ and, for convenience, we omitted the superscript.

Rescaled variables and parameters are summarized in Table 2.2. We remark that α is plant basal mortality rate relative to growth rate; β is a composite dimensionless parameter that measures the impact of toxic compounds on inflation of plant mortality, combining the plant sensitivity s (per unit of concentration of toxic compounds), with typical biomass concentration of toxic compounds cB_{max}, and typical duration of such toxic influence (k^{-1}). Finally, γ measures the characteristic rate of toxicity dynamics relative to plant growth rate.

Table 2.1. List of model parameters and their units.

Parameter	Description	Unit	Assigned value
g	Growth rate of B	month^{-1}	0.5
B_{max}	Plant biomass carrying capacity	kg cm^{-2}	1
d	Death rate of B	month^{-1}	0.05
s	Plant sensitivity to T	cm^2 kg^{-1} month^{-1}	Between 0.15 and 1
D	Plant biomass propagation coefficient	cm^2 month^{-1}	0.05
k	Decay rate of T	month^{-1}	Between 0.05 and 0.2
c	Proportion of toxic products by litter decomposition	-	0.5

Table 2.2. Definitions of the nondimensional variables and parameters appearing in Eq. (2) in terms of their dimensional counterparts.

Quantity	Scaling
$\widetilde{B}$	B/B_{max}
$\widetilde{T}$	Tk/cdB_{max}
$\widetilde{x}$	$x(g/D)^{1/2}$
$\widetilde{y}$	$y(g/D)^{1/2}$
$\widetilde{t}$	gt
α	d/g
β	csB_{max}/k
γ	k/g

3. Results

3.1. Stability analysis of the spatially homogeneous equilibria

The first step in studying the patterns of system (2) is to determine the equilibria of the spatially homogeneous system

$$\begin{cases} \dfrac{dB}{dt} = B(1 - B) - \alpha B(1 + \beta T), \\ \dfrac{dT}{dt} = \gamma B(1 + \beta T) - \gamma T, \end{cases} \tag{3}$$

i.e., the solution of the algebraic equations

$$\begin{cases} B(1 - B) - \alpha B(1 + \beta T) = 0, \\ \gamma[B(1 + \beta T) - T] = 0. \end{cases} \tag{4}$$

Biologically feasible equilibrium points are the non-negative solutions of (4) in the interior of the first quadrant. System (3) has at most two equilibria depending on the magnitude of parameter α:

- if $\alpha \geq 1$ we have only the trivial equilibrium (0,0);
- if $0 < \alpha < 1$, in addition to (0,0), we have the following equilibrium

$$(B_*, T_*) = \left(\frac{(1+\beta) - \Gamma}{2\beta}, \frac{(\beta - 1) - 2\alpha\beta + \Gamma}{2\alpha\beta^2} \right),$$

where

$$\Gamma = \sqrt{(\beta - 1)^2 + 4\alpha\beta}.$$

The Jacobian matrix $J(B,T)$ for system (3) is given by

$$J(B,T) = \begin{pmatrix} 1 - \alpha - 2B - \alpha\beta T & -\alpha\beta B \\ \gamma + \beta\gamma T & -\gamma + \beta\gamma B \end{pmatrix},$$

and at the steady-state $(0,0)$ admits the eigenvalues $\lambda_1 = 1 - \alpha$, $\lambda_2 = -\gamma$. Moreover, at the steady-state (B_*, T_*) the Jacobian matrix J_* has two eigenvalues with negative real parts (see Appendix A). Then, the linear analysis of stability allows us to recognize that for any positive values of parameters β, γ we have:

- the equilibrium $(0,0)$ is asymptotically stable if $\alpha > 1$, unstable if $0 < \alpha < 1$, and consequently $\alpha = 1$ is a bifurcation value;
- the equilibrium (B_*, T_*) is always asymptotically stable for any value of $\alpha : 0 < \alpha < 1$.

This analysis shows that the model has two homogeneous stationary solutions representing bare soil and uniform vegetation cover. Figure 2.3 shows the non-trivial equilibrium values (B_*, T_*) versus β, for some fixed values of plant basal mortality rate relative to growth rate (α). Recalling that $\alpha = d/g$, the existence and the stability character of the equilibria are ecologically consistent. In fact, if the plants death rate d is higher that the growth rate g, the only possible solution is the complete loss of vegetation cover. On the other hand, if the growth rate is higher than the death rate, the biomass stabilizes in a long time on the uniform value B_*.
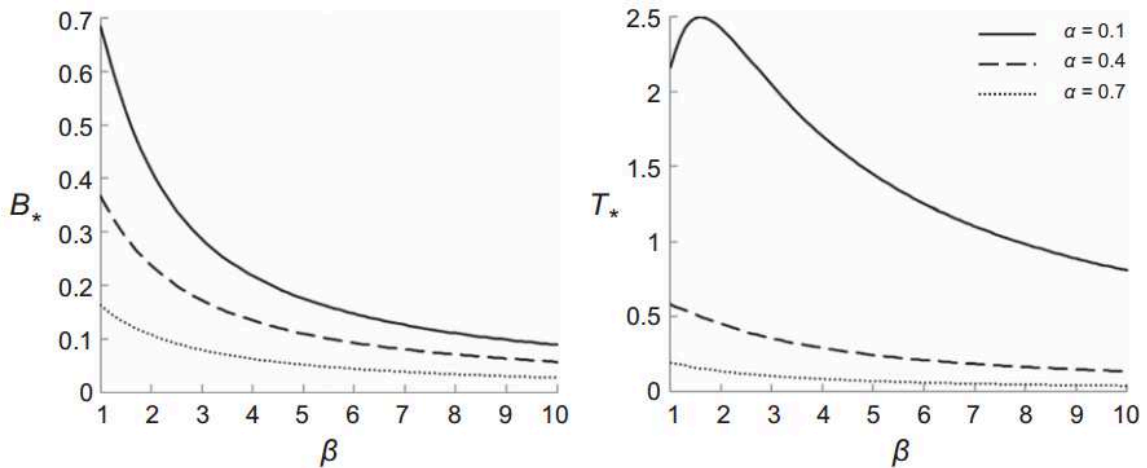
Figure 2.3. Spatially homogeneous equilibria of B (left panel) and T (right panel) versus β, for three different plant species: $\alpha = 0.1$ (solid line), $\alpha = 0.4$ (dashed line) and $\alpha = 0.7$ (dotted line). At low levels of impact of toxic compounds (β) both the equilibria of plant biomass and toxicity are high, i.e., the equilibria decreasing as β increases.

3.2. Linear stability analysis to spatially heterogeneous perturbations

To study the effect of diffusion on the model system, we perform the linear stability analysis of the stationary homogeneous solution (B_*, T_*) of the spatial model (2) to nonuniform infinitesimal perturbations. We consider the perturbed solutions

$$B(\mathbf{r}, t) = B_* + a_B(t)e^{i\mathbf{r}\cdot\mathbf{h}} + cc,$$
$$T(\mathbf{r}, t) = T_* + a_T(t)e^{i\mathbf{r}\cdot\mathbf{h}} + cc, \qquad (5)$$

where $\mathbf{r} = (x,y)$, $\mathbf{h} = (h_1, h_2)$ is the wave vector of the perturbation, $\mathbf{a}(t) = (a_B(t), a_T(t))$ is the vector of the perturbation amplitudes and "cc" stands for the complex conjugate.

Substituting the Eqs. (5) into (2) and keeping terms to first-order only, we obtain the following system of linear ODEs for the perturbation amplitudes $\mathbf{a}(t)$

$$\begin{cases} \dfrac{da_B}{dt} = \left(1 - 2B_* - h - \alpha - \alpha\beta T_*\right)a_B - \alpha\beta B_* a_T, \\[2mm] \dfrac{da_T}{dt} = (\gamma + \beta\gamma T_*)a_B + (-\gamma + \beta\gamma B_*)a_T, \end{cases}$$

$$(6)$$

where $h = |\mathbf{h}|$ is the perturbation's wave number.

Assuming exponential growth for the perturbation amplitudes, i.e.,

$$a_B(t) = B(0)e^{\lambda t},$$
$$a_T(t) = T(0)e^{\lambda t}, \qquad (7)$$

we obtain the eigenvalue problem

$$J(h)\mathbf{a} = \lambda\mathbf{a}, \qquad (8)$$

where $J(h)$ is the coefficient matrix of (6). The solutions $\lambda = \lambda(h)$ of (8) gives the dispersion relations, i.e., provide information about the stability of the stationary homogeneous solution (B_*, T_*). In fact, the growth rate of a perturbation characterized by a wave number h is given by the largest real part of $\lambda = \lambda(h)$. In our case, when $0 < \alpha < 1$ and the coefficients β and γ are positive, all wave numbers have negative growth rates and any perturbation decays, i.e., the uniform solution is asymptotically stable (see Appendix B). In ecological terms, these results show that for $0 < \alpha < 1$, and β, γ, positive parameters, pattern formation always leads to spatially uniform vegetation covers (B_*), and stable Turing patterns cannot exist.

3.3. Travelling fronts

Finally, we examine the system's dynamics when the initial conditions of system (1) are finite, i.e.,

$$B(x,y,0) = \varphi(x,y), \qquad T(x,y,0) = \psi(x,y), (x,y) \in \Omega$$

where φ and ψ are suitable functions with a finite support in the planar domain Ω. In this case, our model, as for some reaction-diffusion models, produce travelling waves of the plant biomass B that travel at velocity $c(t)$ approaching the asymptotic speed

$$c_\infty = \sqrt{4D(g - d)}. \qquad (9)$$

15

In effect, the simple equation for asymptotic invasion velocity for the Fisher model is not restricted to logistic population growth, but more generally arises as

$$c_\infty = \sqrt{4DF'(0)}.$$

(10)

where $F(B)$ is a general class of population growth functions (Holmes *et al.* 1994). In our case, the asymptotic speed c_∞ of the travelling wavefronts, can be obtained easily from heuristic arguments (Volpert and Petrovskii 2009). In fact, at the position of the biomass front, the toxic compounds T is absent and hence this is a problem effectively described by a single KPP-Fisher equation (Kolmogorov *et al.* 1937; Fisher 1937); its speed therefore being given by (10), where

$$F(B) = (g-d)B - \frac{g}{B_{max}}B^2.$$

Owing to relation (9), we can conclude that the asymptotic "invasion velocity" of the biomass B is determined only by the rates of net population growth $(g - d)$ and diffusion D. Since the "coexistence" steady state (B_*, T_*) is locally stable against a nonuniform infinitesimal perturbation, the front is a narrow region that moves with constant shape and speed (Fig. 2.4). As can be better seen in Figure 2.5, a circular invasion front spreads out from the point at which the plant biomass is initially localized, then the area inside the front is populated by plant biomass according to the intensity of the negative feedback (synthetically represented by the dimensionless parameter $\beta=(csB_{max})/k$) produced by T. Consequently, an increase in the impact of toxic compounds on plant mortality (i.e., an increase in the plant sensitivity to autotoxicity s or a decrease in toxic compounds decay/removal rate k), produces a decrease in the equilibrium values as well as a decrease in height and width of the external biomass peaks (Fig. 2.6). Interestingly, for sufficiently high values of β, secondary concentric rings are formed within the patch (Figs. 2.5 and 2.6). As previously described in section 3.2, it has to be remembered that, for long times, inside all the ring patterns there will always be a spatially uniform region with plant biomass and toxic compounds at their coexistence values (B_*, T_*) (Fig. 2.3).
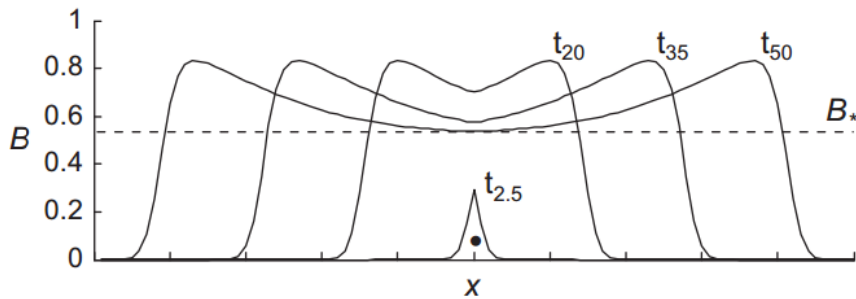
Figure 2.4. Biomass travelling waves. Solid lines represent snapshots from subsequent times from the initial spot centre of B (denoted by •). Lines are obtained as cross-sections of two dimensional simulations of the model equations (Eq. 2). The wavefronts proceed at constant speed (Eq. 9) from the initial spot while the biomass in the centre of the ring slowly approaches the equilibrium value B_* (dashed line). Simulation parameters: $\alpha = 0.1$, $\beta = 1.5$, $\gamma = 0.1$.

16
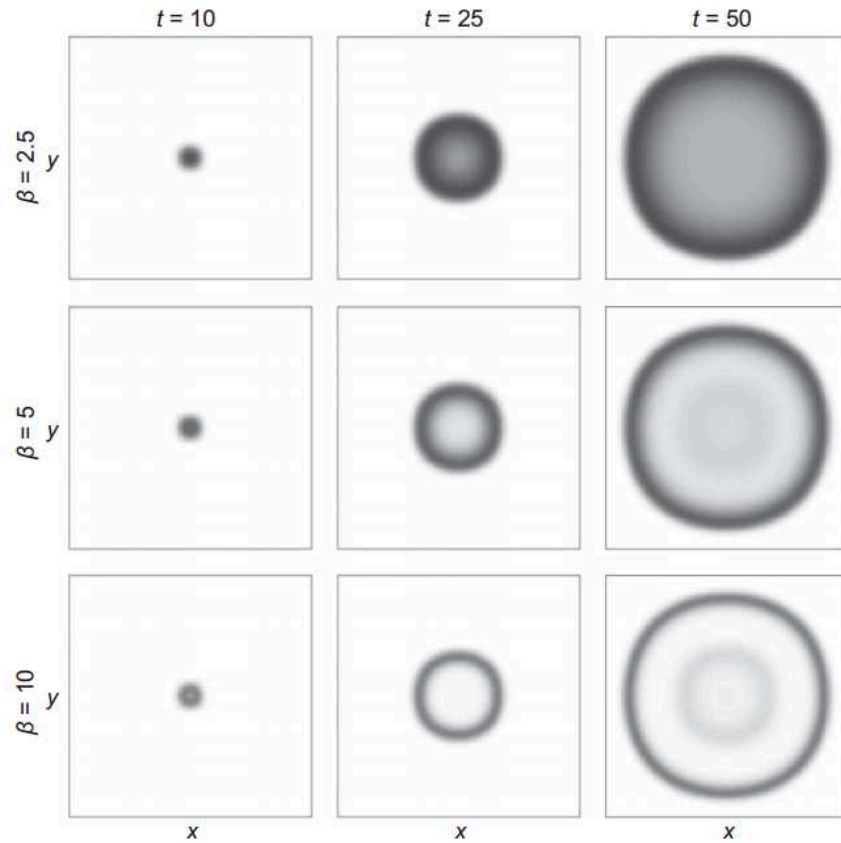
Figure 2.5. Comparison of model simulations (rows) at different values of β, obtained by numerical integration of the model equations (Eq. 2). Each panel shows a grey-scale map of biomass distribution with darker shade representing higher biomass density. Time proceeds from left to right. Other simulation parameters: $\alpha = 0.1$, $\gamma = 0.1$.
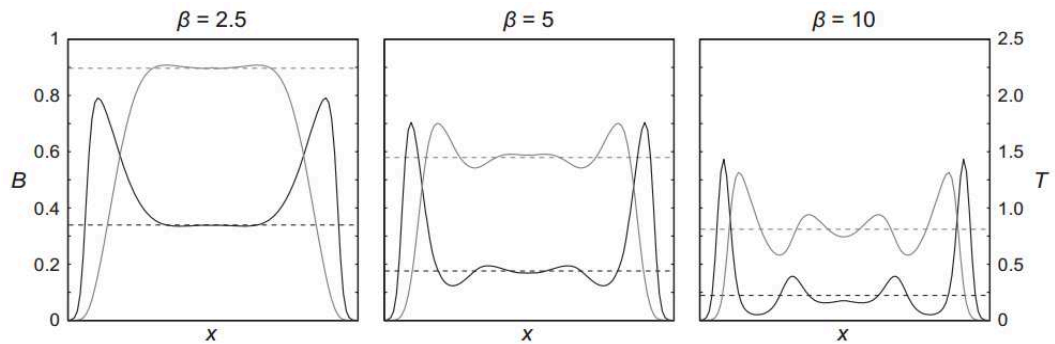
Figure 2.6. Model simulations showing responses of biomass and toxicity distribution along a central transect view across the clonal patch, according to different values of β. The profiles are cross-sections of two dimensional simulations of the model equations (Eq. 2). Each panel shows the distributions of B (solid black line) and T (solid grey line) compared to their equilibrium values B_* (dashed black line) and T_* (dashed grey line). All simulations run for 50 time steps. Other simulation parameters: $\alpha = 0.1$, $\gamma = 0.1$.

4. Discussion

Previous modelling studies related the formation of rings by clonal plants to a resource shortage, i.e., water in arid ecosystems (Rietkerk *et al*. 2002; Gilad *et al*. 2007; Sheffer *et al*. 2007; von Hardenberg *et al*. 2010) which cannot explain the occurrence of ring forming plants when water is not a limiting factor. In particular, such models are based on scale-dependent positive and negative feedbacks between biomass and water (Rietkerk and van de Koppel 2008). Vegetation reduces the presence of soil-crust that inhibits water infiltration and produces shading that reduces soil water evaporation. This set of processes give rise to a positive feedback of vegetation on itself due to the increased water uptake that is only limited by the overall water availability of the system (i.e. precipitation). In this context, the biomass depression in the tussock centre, up to the formation of a clear ring, is the result of competition for water by the surrounding plants, constituting the negative feedback. However, experimental evidences for the water depletion hypothesis are not compelling. For instance, Sheffer *et al*. (2007), studying the grass *Poa bulbosa,* found in a greenhouse experiment that seedlings allocate more biomass to the external tillers, compared to internal ones, as water availability decreases. Indeed, evidence that water depletion occurs inside the rings in open field was not provided. Later, Ravi *et al*. (2008) proposed that the rings of the bunchgrass *Bouteloua gracilis* in semiarid grassland, emerge due to the co-occurring effects of aeolian deposition, changes in soil property inside the clones and water limitation. Specifically, the authors reported that water soil infiltration capacity and water content were slightly, but significantly, reduced inside small and medium size tussocks in the field. However, the difference in soil water content was very small compared to the outwards vegetated belt. Further studies should clarify if a water deficit of such entity can kill a drought adapted bunchgrass. On the other hand, some studies reported an higher water holding capacity in the die-back zone of the ring shaped clones because of the higher organic matter content and changes of soil texture with an higher content of the clay fraction (Pemadasa 1981; Pignatti 1997; Bonanomi 2002; Lanta *et al*. 2004). In conclusion, water depletion may be a factor in the formation of rings in arid systems, but further evidences are required to clarify if this process may explain the formation of rings in ecosystems where water is not a limiting factor. In contrast with the previously described models, our formulation is based on a negative feedback only. The decomposition of biomass produces an increase in soil negative conditions that means a negative effect of vegetation on itself. Our model shows that this type of plant-soil negative feedback can be an additional mechanism responsible for the formation of rings and the appearance of other vegetation patterns in clonal plants. Moreover, compared to previous works on ring formation, the spatial patterns expected by our model are, in a limited interval of time, inhomogeneous states, always leading to long term homogeneous equilibria and uniform vegetation, in contrast with models proposed by Rietkerk *et al*. (2002) and Gilad *et al*. (2007) that provide, for some set of parameters, stationary Turing patterns.
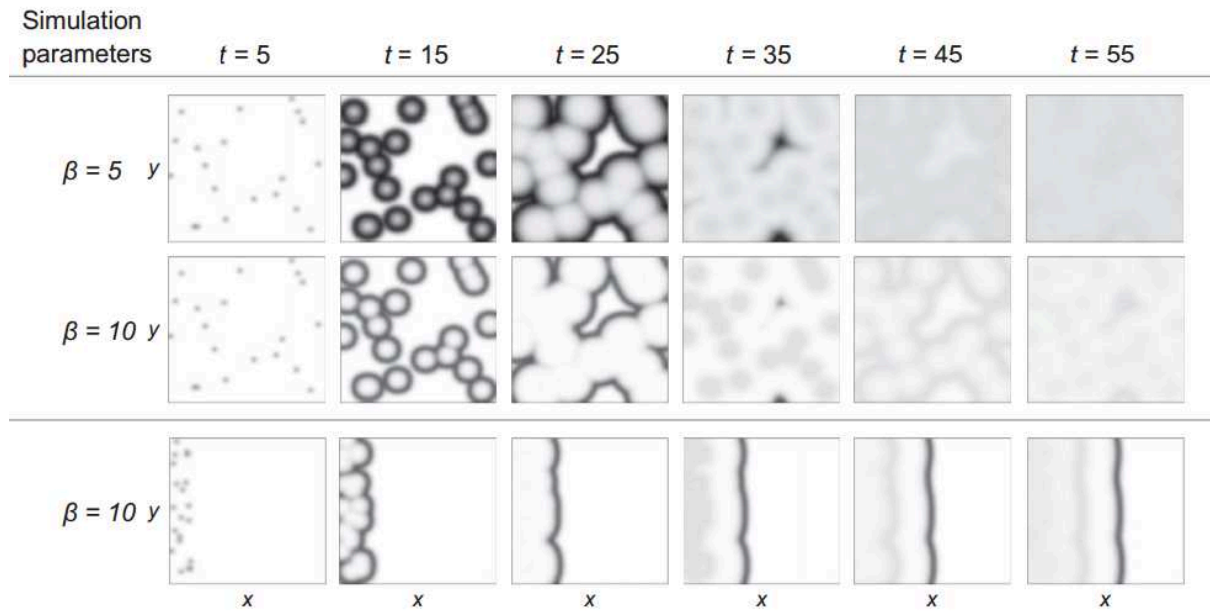
Figure 2.7. Comparison of three model simulations (rows) obtained by numerical integration of the model equations (Eq. 2), initialized with 20 spot-like patches randomly distributed over either the entire domain (first two rows) or the first 10 columns of the lattice (last row), at two different levels of β. Each panel shows a grey-scale map of biomass distribution, with darker shade representing higher biomass density. Time proceeds from left to right. Other simulation parameters: $\alpha = 0.1$, $\gamma = 0.1$.

This model output is actually reflecting real world dynamics, where clear rings are observed only in scattered plants with other patterns becoming evident at higher soil cover levels. In fact, clonal rings have been often reported during colonization of bare substrates in primary successions. Examples include peatland (Lanta *et al*. 2008), volcanic slope (Adachi *et al*. 1996) and salt marsh mud (Caldwell 1957; Castellanos *et al*. 1994). In these conditions, new recruitments occur in an empty space without competition (Caldwell 1957), thus forming clones of regular shape. Similarly, the model provided regular shaped rings after colonization of an empty simulation grid followed, when the clones develop and come into contact with other patches, by their progressive disappearance with subsequent coalescence as observed in nature (Watt 1947; Heslop-Harrison and Heslop-Harrison 1958). Interestingly, the disappearance of regular patterns after rings coalescence has been observed also for fungal "fairy rings" when underground mycelia of neighbouring rings come into contact (Dowson *et al*. 1989). However, the mechanisms underlying the spatial rearrangement of vegetative structures during clones coalescence are unknown. Keeping in mind such considerations, it seems clear that the occurrence of either rings or other patterns, such as wave-like structures, during the colonization of bare substrates, is dependent on the initial arrangement of plant recruitment. Simulations shown in Figure 2.7 (first two rows) indicate that randomly distributed plant patches do produce regularly shaped rings or part of rings if new patches are initially enough spaced (i.e. the distance between their establishment locations is larger than the average adult patch diameter), progressively disappearing with rings contact and coalescence. On the other hand, if initial recruitment occurs in clusters or along a line (last row of Fig. 2.7), e.g. in a grassland colonization from a woodland edge, different patterns may

emerge as wave-like bands. A real pattern similar to that obtained at intermediate stages of our simulation, showing semi-rings waves, has been reported in herbaceous grasslands and related to the build-up of species-specific negative feedback (Blomqvist *et al*. 2000; Olff *et al*. 2000). In such communities, dominant species move away from "home" soil by vegetative propagation, to escape accumulated soil-borne pathogens. Likely, in these cases regular rings do not emerge because all soil is covered and each plant may expand only into spaces released by other species when they are affected by their own negative feedback. Indeed, further modelling attempts might investigate the effects of species-specific negative feedback on the spatial arrangement of multi-species plant assemblages.

Model analysis showed that the negative feedback intensity (parameter β) strongly affects the biomass production in the central tussock zone, ranging, with increasing β, from a slight reduction of central shoots, to a complete die-back, to bare soil. This variability in degeneration levels of the internal ring zone has been reported in natural ecosystems. For instance, Bonanomi and Allegrezza (2004) reported, in the case of the ring forming grass *B. rupestre*, both small reductions and complete absence of biomass in the central parts of different clones in four different study sites. Recently, Otfinowski (2008) also found only a small reduction of living biomass in the centre of *B. inermis* clones. In contrast, many studies reported completely empty central areas of most investigated rings (Watt 1947; Curtis and Cottam 1950; Caldwell 1957; Castellanos *et al*. 1994; Danin 1996; Lewis *et al*. 2001; Bonanomi, Rietkerk, *et al*. 2005). These observations are consistent with the large variability of experimentally observed negative plant-soil feedback intensity, ranging from small reductions of plant growth to lack of regeneration of conspecific individuals (Packer and Clay 2000; Klironomos 2002; Kardol *et al*. 2007; Mazzoleni *et al*. 2007; Kulmatiski *et al*. 2008). We also suggest that an elevated negative feedback intensity, resulting from high plant sensitivity coupled with low levels of removal/decay rates of toxic compounds, may well explain the development of concentric rings within the same clone. This rarely observed pattern (Caldwell 1957; G. Bonanomi, *pers. obs.*), appeared in our model simulations if the plant suffered strong negative feedback with, at the same time, the toxicity slowly disappearing from the affected soil. Under these conditions, several concentric waves of vegetative propagation can develop in the absence of interspecific competition because the soil can be re-colonized by the same species as soon as the detrimental effect of negative feedback is decreased. Experimental studies are needed to test the consistency of this hypothesis.

In conclusion, our simple single-species model demonstrates that negative plant-soil feedback due to toxicity by the decomposition processes of accumulated litter may well explain the formation of differently shaped rings and of vegetation waves during substrate colonization. Previous models (Sheffer *et al*. 2007; von Hardenberg *et al*. 2010) were also able to reproduce clonal rings, but only in arid, water-limited ecosystems. Far from stating that plant-soil negative feedback is the only process involved in the formation of vegetation patterns, an interesting development on this topic could be the formulation of a model that considers the integration of both mechanisms (plant-water and plant-soil toxicity feedbacks), in order to evaluate the relative importance of such processes in different environmental conditions. Moreover, a multi-species model, with species-specific negative plant-soil feedback, can be developed for better understanding plant species distribution in space and time.

Future manipulative field experiments are certainly strongly required to test specific hypotheses and to clarify the mechanisms underlying ring formation. In particular, the water limitation hypothesis could be verified by irrigating the central part of the rings to check if this would allow a centripetal recolonization by the clonal plant. On the other hand, the investigation of the toxicity hypothesis should imply a clarification of the mechanisms producing plant-soil negative feedback which has been attributed to nutrient depletion (Ehrenfeld *et al*. 2005), soil-borne pathogens (Packer and Clay 2000), soil microbial communities (Klironomos 2002) and autotoxicity produced by litter decomposition (Singh *et al*. 1999). Fertilization experiments could be used to test the role of nutrient levels in ring formation, whereas, comparative chemical and microbial characterization of the inner and outer zones of the clonal rings in the field should be performed to assess the other mechanisms. In particular, following previous research work (Bonanomi, Incerti, *et al*. 2011), further detailed studies by NMR-CPMAS methods could address this critical issue, with experiments being specifically designed to support the autotoxicity theory.

Acknowledgements

Appendix A

The non-negative uniform steady-state (B_*, T_*) is asymptotically stable if and only if $0 < \alpha < 1$ and the parameters β and γ are positive. In fact, the characteristic equation is given by

$$\lambda^2 - (trJ_*)\lambda + \det J_* = 0,$$

where

$$\det J_* = \frac{-(\beta-1)^2 - 4\alpha\beta + (1+\beta)\sqrt{(\beta-1)^2 + 4\alpha\beta}}{2\beta}\gamma,$$

$$trJ_* = -\frac{1+\beta-(\beta-1)\beta\gamma}{2\beta} - \frac{(\beta\gamma-1)\sqrt{(\beta-1)^2 + 4\alpha\beta}}{2\beta}.$$

After some standard calculations, we derive that $\det J_* > 0$ and $tr J_* < 0$ if and only if $0 < \alpha < 1$ and the parameters β and γ are positive. Then, the Jacobian matrix J_* has two eigenvalues with negative real parts.

Appendix B

The linear stability of the uniform state (B_*, T_*) is deduced from the dispersion relations

$$J(h)\mathbf{a} = \lambda\mathbf{a}, \tag{B.1}$$

where the Jacobian matrix is

$$J(h) = \begin{pmatrix} 1 - \alpha - 2B_* - \alpha\beta T_* & -\alpha\beta B_* \\ \gamma + \beta\gamma T_* & -\gamma + \beta\gamma B_* \end{pmatrix}.$$

Indeed, the Eq. (B.1) can be written as

$$\lambda^2 - (trJ(h))\lambda + \det J(h) = 0,$$

where

$$\det J(h) = \det J_* + \frac{1}{2}h\left(1 - \beta + \sqrt{(\beta-1)^2 + 4\alpha\beta}\right)\gamma,$$

$$trJ(h) = trJ_* - h.$$

Then, (B_*, T_*) is asymptotically stable if and only if the matrix $J(h)$ has two eigenvalues with negative real parts. Owing to $h > 0$, the stability condition takes the following form:

$$\det J(h)_* > 0,$$
$$\text{tr } J(h)_* < 0,$$

which holds if $0 < \alpha < 1$ and the parameters β and γ are positive.

3

VEGETATION PATTERN FORMATION: A BALANCE BETWEEN WATER AND TOXICITY FEEDBACKS

―――――――――――――――――――――――――

Addolorata Marasco, Annalisa Iuorio, Fabrizio Cartenì, Giuliano Bonanomi, Stefano Mazzoleni, Francesco Giannino.

Abstract

The formation of vegetation patterns has been widely analyzed and discussed over the years and, generally, it has been related to biomass-water feedbacks. In this work, we study the mechanisms underlying vegetation pattern formation as a result of both positive feedback between biomass and water and negative plant–soil feedback due to the presence of toxic compounds. The proposed model exhibits different spatial patterns, although Turing conditions are not satisfied, and the distribution of biomass within the patterns is not symmetrical as predicted by other models. Furthermore, we show that, in case of high persistence of toxicity in the soil, spatial patterns are continuously moving in space without reaching a stable spatial configuration.

1. Introduction

The occurrence of regular patterns of vegetation has been studied by plant ecologists for a long time (Watt 1947; White 1971). Different patterns, such as spots, labyrinths, gaps and stripes as well as plant rings and fungal fairy rings (Valentin *et al*. 1999; Bonanomi *et al*. 2012, 2013) have been reported in a variety of natural environments (Boaler and Hodge 1964; Wickens and Collier 1971; Leprun 1999; Okayasu and Aizawa 2001). Recently Deblauwe *et al*. (2008), by studying 249 geographical locations, have explained the occurrences of regular patterns by means of climatic variables and soil properties. The interest for vegetation pattern formation is related to the comprehension of local and global phenomena like climate change (Rietkerk *et al*. 2002; Dekker *et al*. 2010). In particular, the study of vegetation patterns in arid and semi-arid environments could provide useful tools to identify early warning signals for climate shifts and critical transitions (Rietkerk *et al*. 1997, 2004; van de Koppel *et al*. 1997; Scheffer *et al*. 2009). Several feedback mechanisms have been proposed to explain the formation of vegetation patterns, and many mathematical models have been formulated to test these hypotheses (Rietkerk and van de Koppel 2008; Meron 2010; Zelnik *et al*. 2013).

Starting from the analysis of biomass evolution, Lefever and Lejeune (Lefever and Lejeune 1997) developed a phenomenological model which ascribes vegetation patterns to two feedbacks: short-range facilitation of plants under their aerial structures, and long-range competition between plants by overlapping root zones (Lejeune *et al*. 1999, 2002). A huge part of the scientific literature, however, identifies water as the main causal factor for the emergence of vegetation patterns. These models are usually written in terms of partial differential equations (PDEs) reproducing the dynamics of water and plant biomass. The first model, based on two equations, was introduced by Klausmeier (1999). In this model, the formation of patterns derives from two main processes: short range facilitation of plants on themselves, and long range inhibition due to shortage of available water. Following Klausmeier's work, several authors modelled water as two separate state variables, soil and surface water (von Hardenberg *et al*. 2001; Rietkerk *et al*. 2002; Meron *et al*. 2004, 2007; Ursino and Contarini 2006; Gilad *et al*. 2007; Nathan *et al*. 2013). The outcome of these models still shows that the occurrence of vegetation patterns is strictly connected with feedbacks between biomass and water, such as water infiltration, evaporation, plant uptake and surface runoff. On the other hand, the formation of vegetation patterns can hardly be explained in humid environments (Rietkerk and van de Koppel 2008 and references therein) if water is assumed to be the only responsible factor. Therefore, the *plant-soil negative feedback* (NF) hypothesis (Mazzoleni *et al*. 2007) has been used to justify the emergence of ring vegetation patterns (Carteni *et al*. 2012). Species-specific NF has been defined as the raise of negative conditions for plants induced by the accumulation in the soil of toxic compounds released by decomposing litter of the same plant species. The presence of soil-borne pathogens, the changing composition of soil microbial communities (Kulmatiski *et al*. 2008), and the accumulation of autotoxic compounds from decomposing plant litter (Bonanomi, Incerti, *et al*. 2011) are just some of the mechanisms involved in the plant-soil negative feedback. So far, this phenomenon has been proved to play an important role in plant species coexistence as in biodiversity (Mazzoleni *et al*. 2010). Following this hypothesis, another model, consisting of two partial differential equations (PDEs) for biomass and toxicity, has been proposed to explain the occurrence of ring patches in clonal plants (Carteni *et al*. 2012). Moreover, Marasco *et al*. (2013) have recently introduced a new model formulation for vegetation pattern formation based on the interactions between water and plant-soil negative feedback. According to the numerical simulations, although without a solid mathematical analysis of the underlining PDEs, the model shows the ability to reproduce the emergence of vegetation patterns even when water is not a limiting resource.

Spatial patterns are often defined as *Turing patterns* named after Alan Turing who first proposed the regular pattern formation by scale-dependent feedbacks in chemical and

biological systems (Turing 1952). Such patterns arise from the so-called activator-inhibitor principle in chemical (Rovinsky and Menzinger 1993; Jensen *et al*. 1994; Coullet *et al*. 2000), physical (Tlidi *et al*. 1994; Kessler and Werner 2003), and biological systems (Meinhardt 1995; Murray 2002). In particular, the mechanism at the base of Turing vegetation patterning is the difference between the diffusion rates of plant biomass and water, with the latter being sensibly higher. In mathematical terms, a reaction-diffusion system exhibits Turing patterns if the stability of an homogeneous steady state is lost with respect to heterogeneous perturbations. In many cases, however, dynamical models reveal the presence of vegetation patterns even when this condition is not satisfied (Petrovskii *et al*. 2001; Volpert and Petrovskii 2009; Kéfi *et al*. 2010). In Kéfi *et al*. (2010), this case is explained as the emergence of *non-Turing patterns*. Moreover, Petrovskii *et al*. (2001) highlighted an interesting phenomenon which leads to pattern formation called *dynamical stabilization*. This phenomenon describes the formation of an unstable plateau behind the diffusive front, due to *"the interplay between the diffusion and nonlinear inter-species interactions"* (Petrovskii *et al*. 2001). The dynamical stabilization appears opposite to the mechanisms of Turing pattern formation.

In this paper, we study the mechanisms underlying the vegetation pattern formation as a result of both positive and negative feedbacks between biomass and water, and negative plant-soil feedback due to the presence of the toxic compounds. Performing a suitable nondimensional analysis, differently to Marasco *et al* (2013), we introduce new dimensionless variables and model parameters that allow us to simulate the emergence of the vegetation patterns with realistic values of precipitation. The resulting PDEs system exhibits stable spatial patterns although Turing conditions are not satisfied. In addition, we show that in case of high persistence of toxicity in the soil, the generated spatial patterns are continuously moving in space. Numerical simulations also highlight that the distribution of biomass within the patterns, is not symmetrical as predicted by other models (Rietkerk *et al*. 2002; Meron *et al*. 2004, 2007; Gilad *et al*. 2007).

The paper is organized as follows. In Section 2 we define the mathematical model in dimensional and nondimensional form. Section 3 is devoted to the linear stability analysis to spatially homogeneous and heterogeneous perturbations. In order to compare our results with the ones presented in the Klausmeier's work (1999), the same analysis was also carried out assuming no toxicity effects on biomass dynamics. In addition, we perform a bifurcation analysis on some characteristic parameters. Finally, numerical simulations are performed in order to illustrate the evolution of these patterns in time, and the influence of toxicity on biomass dynamics. In Section 4, we conclude discussing the ecological and mathematical implications of our results.

2. The mathematical model

To explain the occurrence of vegetation patterns under different environmental conditions, we present a differential system that models the positive and negative feedbacks among biomass B, water W, and toxic compounds T inspired by Klausmeier (1999), Cartenì *et al.* (2012), and Marasco *et al.* (2013).

As schematically represented in Figure 3.1, we suppose that plant biomass B (kg/m2) grows according to water availability, and its intrinsic mortality (d) is incremented by an extra loss induced by the toxic compounds T (kg/m2). Moreover, the total water content W is affected by rain, evaporation and plant uptake (i.e., transpiration), while the decomposition of dead plants (i.e., litter) produces toxic compounds T that are degraded and removed from the soil according to environmental conditions (such as precipitation and temperature), exerting a negative effect on plant growth performance (Fig. 3.1).

Starting from the model presented in Marasco *et al.* (2013), we develop a different mathematical analysis of the PDEs system showing how the dynamical stabilization phenomenon, occurring in the presence of water limitation and negative plant–soil feedback, allows us to explain vegetation patterns formation that are spatially unstable in time. Moreover, our model exhibits vegetation patterns on flat soil, also when we neglect the negative plant–soil feedback.
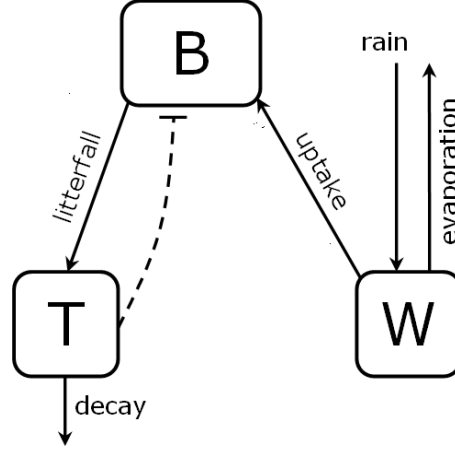
Figure 3.1. Soil-Plant-Atmosphere System. Schematic representation of the feedbacks and interactions among plant biomass (*B*), toxic compounds (*T*) and soil water (*W*). Continuous lines represent transfers of matter between the compartments while dashed lines represent influences.

2.1. Model equations

Plant biomass *B* (representing the whole system of roots and shoots) grows proportionally (*c*) to water availability, its intrinsic mortality (*d*) is incremented by an extra loss induced by the toxic compound *T* by means of a sensibility parameter *s*. The vegetative growth and the seed dispersal is modelled by a diffusion term of coefficient D_B. Furthermore, water *W* representing both soil and surface water, is supplied uniformly due to precipitation at constant rate *p* and lost due to evaporation at rate *lW*; plants absorb water at rate rB^2W, and, finally the transport of water (following the Darcy's law) is modelled by a diffusion term of coefficient D_W. Toxic compounds *T* are produced by a fraction *γ* of the dead biomass, and are reduced by intrinsic decay and water precipitation processes through the parameters *k* and *ε*, respectively.

All the model parameters are summarized in Table 3.1; their values are chosen according to Klausmeier (1999) and Cartenì *et al.* (2012) or set to order-of-magnitude feasible values. The spatial variables are *(x,y)*, while *t* is the time variable.

According to the above hypotheses, the model equations are

$$\begin{cases} \dfrac{\partial B}{\partial t} = cB^2W - (d + sT)B + D_B \Delta B, \\[2mm] \dfrac{\partial W}{\partial t} = p - rB^2W - lW + D_W \Delta W, \\[2mm] \dfrac{\partial T}{\partial t} = \gamma(d + sT)B - (k + \varepsilon p)T, \end{cases} \tag{1}$$

where we assume only positive values for the parameters *c, d, p, r* and *γ*, whereas *l, s, ε, k, D_B, D_W* are non negative.

Introducing the dimensionless variables and parameters

$$\tilde{B} = \frac{kr}{cp}B, \quad \tilde{W} = \frac{k}{p}W, \quad \tilde{T} = \frac{kr}{cp\gamma}T, \quad \tilde{x} = x\left(\frac{k}{D_W}\right)^{1/2}, \quad \tilde{y} = y\left(\frac{k}{D_W}\right)^{1/2}, \quad \tilde{t} = kt$$

$$\alpha = \frac{d}{(k+\varepsilon p)}, \quad \delta = \frac{cps\gamma}{(k+\varepsilon p)^2 r}, \quad \nu = \frac{c^2 p^2}{(k+\varepsilon p)^2 r}, \quad \vartheta = \frac{D_B}{D_W}, \quad \lambda = \frac{l}{(k+\varepsilon p)}, \quad (2)$$

we obtain the following nondimensional model (for convenience, we omit the superscript)

$$\begin{cases} \dfrac{\partial B}{\partial t} = \nu B^2 W - \delta BT - \alpha B + \vartheta \Delta B, \\[2mm] \dfrac{\partial W}{\partial t} = 1 - \nu B^2 W - \lambda W + \Delta W, \\[2mm] \dfrac{\partial T}{\partial t} = \alpha B - T + \delta BT, \end{cases} \quad (3)$$

where α can be interpreted as the intrinsic death rate, obtained balancing the plant mortality rate and the toxicity loss velocity $k+\varepsilon p$ (depending on the decay parameter k and the rain washing effect εp). δ is an extra death rate directly proportional to the parameters controlling plant growth (i.e., growth rate c and rain p) and plant mortality (i.e., toxic compounds released from a fraction γ of dead biomass and its sensibility s to toxicity), and inversely proportional to the toxicity loss velocity $(k+\varepsilon p)$ and to water uptake r. The parameter ν is the ratio between the parameters controlling plant growth and the product of toxicity loss velocity and water uptake. Finally, λ is the ratio of the water loss parameter l on toxicity loss velocity, and ϑ is the ratio between biomass and water diffusion coefficients.

Table 3.1. List of model parameters

Parameter	Description	Unit	Assigned Value
c	Growth rate of B due to water uptake	$m^4 \, day^{-1} \, kg^{-2}$	0.002
d	Death rate of B	day^{-1}	0.01
s	Plant sensitivity to T	$m^2 \, kg^{-1} \, day^{-1}$	0 or 0.2
D_B	Plan biomass propagation coefficient	$m^2 \, day^{-1}$	0.01
p	Rainfall	$kg \, day^{-1} \, m^{-2}$	Between 0 and 2
r	Water uptake due to biomass growth	$m^4 \, day^{-1} \, kg^{-2}$	0.35
l	Water loss due to evaporation and drainage	day^{-1}	0.01
D_W	Water diffusion coefficient	$m^2 \, day^{-1}$	0.8
γ	Proportion of toxic products by litter decomposition	-	0.05
k	Decay rate of T	day^{-1}	0.01 or 0.2
ε	Washing effect due to precipitation	$kg \, day^{-2} \, m^{-2}$	0.001

3. Results

In this section, we perform a stability analysis of the spatially homogeneous equilibria of Eqs. (3), and we draw the bifurcation diagrams of biomass, with rainfall p as a bifurcation parameter, for different values of k and s. In addition, we numerically integrate Eqs. (3) fixing the values of all the dimensional parameters except the precipitation p, the sensibility s, and the decay rate k of T. Moreover we numerically investigate both the effects of initial biomass condition and rain parameter p.

3.1 Stability analysis of the spatially homogeneous equilibria

We perform a stability analysis of the spatially homogeneous equilibria in two cases:

a) the parameter s and consequently the non-dimensional parameter δ is strictly positive, i.e., we assume that the negative plant–soil feedback affects biomass dynamics;

b) the parameter s and consequently δ are zero, i.e., the biomass and water equations in (3) are decoupled with respect to the toxic compounds T, then the resulting biomass–water differential system becomes equivalent to Klausmeier's model on flat soil.

Case a): $s \neq 0$ therefore $\delta \neq 0$

In the first stage we find the stationary solutions of the spatially homogeneous system, i.e., the solutions of the system

$$\begin{cases} \nu B^2 W - \delta BT - \alpha B = 0, \\ 1 - \nu B^2 W - \lambda W = 0, \\ \alpha B - T + \delta BT = 0, \end{cases} \tag{4}$$

Biologically feasible equilibrium points are the non-negative solutions of the above system, i.e.,

if $\lambda > 0 \Rightarrow (B_1, W_1, T_1) = \left(0, \dfrac{1}{\lambda}, 0\right)$;

if $\lambda = 0 \Rightarrow (B_2, W_2, T_2) = \left(\dfrac{1}{\alpha + \delta}, \dfrac{(\alpha + \delta)^2}{\nu}, 1\right)$;

if $0 < \lambda \leq \dfrac{\nu}{4\alpha^2 + 4\alpha\delta} \Rightarrow$

$$(B_3, W_3, T_3)^- = \left(\dfrac{\nu - \sqrt{\nu(-4\alpha(\alpha + \delta)\lambda + \nu)}}{2(\alpha + \delta)\nu}, \dfrac{2\delta(\alpha + \delta)\lambda + \nu + \sqrt{\nu(-4\alpha(\alpha + \delta)\lambda + \nu)}}{2\lambda(\delta^2\lambda + \nu)}, \dfrac{-2\alpha\delta\lambda + \nu + \sqrt{\nu(-4\alpha(\alpha + \delta)\lambda + \nu)}}{2(\delta^2\lambda + \nu)}\right),$$

$$(B_3, W_3, T_3)^+ = \left(\dfrac{\nu + \sqrt{\nu(-4\alpha(\alpha + \delta)\lambda + \nu)}}{2(\alpha + \delta)\nu}, \dfrac{2\delta(\alpha + \delta)\lambda + \nu - \sqrt{\nu(-4\alpha(\alpha + \delta)\lambda + \nu)}}{2\lambda(\delta^2\lambda + \nu)}, \dfrac{-2\alpha\delta\lambda + \nu + \sqrt{\nu(-4\alpha(\alpha + \delta)\lambda + \nu)}}{2(\delta^2\lambda + \nu)}\right),$$

The Jacobian matrix $J(B, W, T)$ associated to system (3) is given by

$$J(B, W, T) = \begin{pmatrix} -\alpha + 2BW - \delta T & \nu B^2 & -\delta B \\ -2\nu BW & -\nu B^2 - \lambda & 0 \\ \alpha + \delta T & 0 & \delta B - 1 \end{pmatrix}.$$

Then, the linear analysis of stability allows us to obtain the following results:

i) the equilibrium (B_1,W_1,T_1) (corresponding to bare soil) is asymptotically stable if and only if $\alpha>0$. In fact, the Jacobian matrix at (B_1,W_1,T_1) admits the eigenvalues $\lambda_1=-1$, $\lambda_2=-\lambda$, $\lambda_3=-\alpha$;

ii) at the equilibria (B_2,W_2,T_2) and $(B_3,W_3,T_3)^{\pm}$ (corresponding to uniform vegetation) the stability properties involves all model parameters in a non trivial way. Then, the linear analysis of stability of these equilibria should be examined only on varying the ecologically relevant parameters p and k, whereas for the others we assume that $c=0.002$, $d=0.01$, $s=0.2$, $r=0.35$, $l=0.01$, $D_W=0.8$, $D_B=0.01$, $\gamma=0.05$, $\varepsilon=0.001$, i.e.,

$$\alpha = \frac{10}{(1000k + p)}, \quad \delta = \frac{400p}{7(1000k + p)^2}, \quad \nu = \frac{80000p^2}{7(1000k + p)^2}, \quad \vartheta = \frac{1}{80}, \quad \lambda = \frac{10}{1000k + p}, \quad (5)$$

where from now on, for the sake of simplicity, we omit the parameter units.

Owing to (5), the equilibrium (B_2,W_2,T_2) does not exist (since $\lambda \neq 0$).

We define

$$F(k,p)=-7000k - 47p + 20000kp^2 + 20p^3 \qquad (6)$$

and, for any fixed value $\overline{k}$ of k

$$G(p)=F(\overline{k},p)=-7000\overline{k} - 47p + 20000\overline{k}p^2 + 20p^3 \qquad (7)$$

Then, $(B_3,W_3,T_3)^{\pm}$ exist if and only if $p \geq p^*(\overline{k})$, where p^* is the positive root of the polynomial G(p), and $(B_3,W_3,T_3)^-$ is always unstable, and $(B_3,W_3,T_3)^+$ is always stable to homogeneous perturbations (see Fig. 3.2a-b)

Case b): $s=0$ therefore $\delta=0$

An analogous scenario is obtained assuming that toxicity and biomass dynamics are decoupled, i.e., $\delta=0$. In this case, our model becomes a biomass-water model similar to Klausmeier's model but without soil topographic variations. Once again we will have a bare soil equilibrium $(\overline{B}_1,\overline{W}_1,\overline{T}_1)$ and three possible uniform vegetation equilibria $(\overline{B}_2,\overline{W}_2,\overline{T}_2)$, and $(\overline{B}_3,\overline{W}_3,\overline{T}_3)^{\pm}$ as in Table 3.2.

Fixing the parameters as in (5) (except for δ and s which are now equal to zero), the equilibrium $(\overline{B}_2,\overline{W}_2,\overline{T}_2)$ does not exist (since $\lambda \neq 0$), whereas $(\overline{B}_3,\overline{W}_3,\overline{T}_3)^{\pm}$ exist if and only if $p \geq \frac{1}{2}\sqrt{\frac{7}{5}}$. In fact, in this case neglecting the value of toxicity decay rate k only the parameter p influence biomass dynamics.

Stability analysis to spatially homogeneous perturbations leads us to $(\overline{B}_1,\overline{W}_1,\overline{T}_1)$ and $(\overline{B}_3,\overline{W}_3,\overline{T}_3)^+$ are asymptotically stable equilibria, conversely $(\overline{B}_3,\overline{W}_3,\overline{T}_3)^-$ is always unstable (see Fig. 3.2c).

Owing to the above results, in Section 3.2 we perform a stability analysis to nonuniform infinitesimal perturbations. Moreover, in Figure 3.2 we report three bifurcation diagrams corresponding to the cases $\delta \neq 0$ and $\delta=0$. In the first case, we examine the stability character of the equilibria only when $k=0.01$ (i.e., high presence of toxicity in the soil) and $k=0.2$ (i.e., low presence of toxicity in the soil).
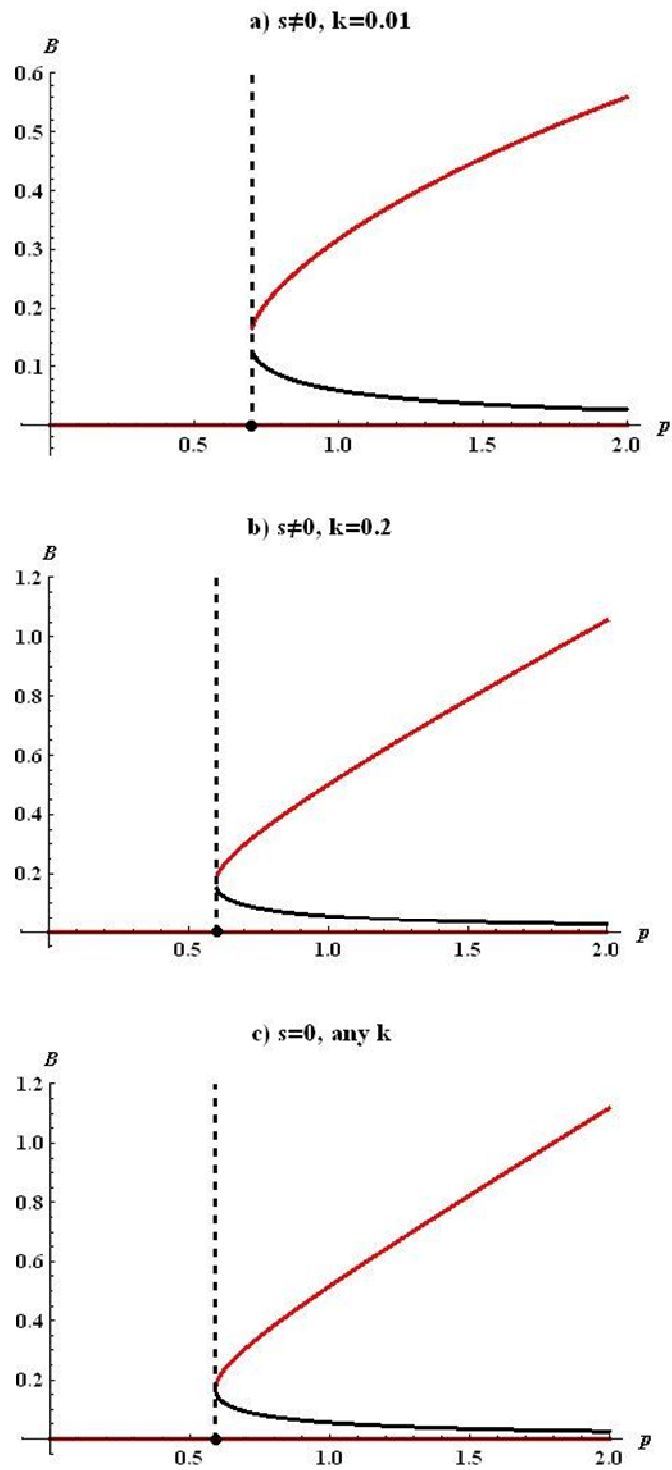
Figure 3.2. Bifurcation diagrams for homogeneous stationary solutions of the model equations (1) showing the biomass B versus the precipitation rate p, for *k=0.01* (panel a) and *k=0.2* (panel b) when *s=0.2* and for any *k* when *s=0* (panel c) . Red lines denote stable equilibria of the spatial and nonspatial model. Continuous lines are unstable equilibria of the nonspatial model. Spatial bistability occurs when *p≥p**.

Table 3.2. Stationary solutions for model equations (2) with different biomass-toxicity dynamics

$\delta \neq 0$	
if $\lambda > 0$	$\left(0, \dfrac{1}{\lambda}, 0\right)$
if $\lambda = 0$	$\left(\dfrac{1}{\alpha+\delta}, \dfrac{(\alpha+\delta)^2}{\nu}, 1\right)$
if $0 < \lambda \le \dfrac{\nu}{4\alpha^2 + 4\alpha\delta}$	$\left(\dfrac{\nu \pm \sqrt{\nu(-4\alpha(\alpha+\delta)\lambda + \nu)}}{2(\alpha+\delta)\nu}, \dfrac{\alpha\delta\lambda + \delta^2\lambda + \nu - \alpha\nu B_1[t_1 x_1 y] - \delta\nu B_3^{\pm}}{\lambda(\delta^2\lambda + \nu)}, 1 - \lambda\alpha W_3^{\pm}\right)$
$\delta = 0$	
if $\lambda > 0$	$\left(0, \dfrac{1}{\lambda}, 0\right)$
if $\lambda = 0$	$\left(\dfrac{1}{\alpha}, \dfrac{\alpha^2}{\nu}, 1\right)$
if $0 < \lambda \le \dfrac{\nu}{4\alpha^2}$	$\left(\dfrac{\nu - \sqrt{-4\alpha^2\lambda\nu + \nu^2}}{2\alpha\upsilon}, \dfrac{1 - \alpha\overline{B_3^{\pm}}}{\lambda}, \alpha\overline{B_3^{\pm}}\right)$

3.2 Linear stability analysis to spatially heterogeneous perturbations

In order to investigate the effect of the biomass and water diffusion on the model system (3) we perform the linear stability analysis of the stationary homogeneous solutions (B_1, W_1, T_1) and $(B_3, W_3, T_3)^+$ to nonuniform infinitesimal perturbations.

We consider the perturbed solutions

$B(\boldsymbol{x}, t) = B_* + a_B(t)e^{i\boldsymbol{x}\cdot\boldsymbol{h}} + cc,$

$W(\boldsymbol{x}, t) = W_* + a_W(t)e^{i\boldsymbol{x}\cdot\boldsymbol{h}} + cc,$

$T(\boldsymbol{x}, t) = T_* + a_T(t)e^{i\boldsymbol{x}\cdot\boldsymbol{h}} + cc,$

where (B_*, W_*, T_*) is a spatially stable equilibrium solution, $\boldsymbol{x}=(x,y)$ is the space variables vector, $\boldsymbol{h}=(h_1, h_2)$ is the wave vector of the perturbation, $a(t)=(a_B(t), a_W(t), a_T(t))$ is the perturbation amplitudes vector and *"cc"* stands for complex conjugate.

Substituting the above perturbed solutions in (3) and keeping terms to first-order only, we obtain the following system of linear ODEs for the perturbation amplitudes $\boldsymbol{a(t)}$:

$$\begin{cases} \dfrac{da_B}{dt} = (-\alpha + 2\nu B_* W_* - \delta T_* - h^2\vartheta)a_B + \nu B_*^2 a_W - \delta B_* a_T, \\[2mm] \dfrac{da_W}{dt} = (-h^2 - 2\nu B_* W_*)a_B - (\nu B_* + \lambda)a_W \\[2mm] \dfrac{da_T}{dt} = (\alpha + \delta T_*)a_B + (\delta B_* - 1)a_T \end{cases} \qquad (8)$$

where $h=|\boldsymbol{h}|$ is the perturbation's wave number.

Assuming exponential growth for the perturbations amplitudes, i.e.,

$$a_B(t) = a_B(0)e^{\lambda t}, \qquad a_W(t) = a_W(0)e^{\lambda t}, \qquad a_T(t) = a_T(0)e^{\lambda t},$$

we obtain the eigenvalues problem

$$J(h)\mathbf{a} = \lambda\mathbf{a}, \tag{9}$$

where

$$J(h) = \begin{pmatrix} -\alpha + 2\nu BW - \delta T - h^2\vartheta & \nu B^2 & -\delta B \\ -h^2 - 2\nu BW & -\nu B^2 - \lambda & 0 \\ \alpha + \delta T & 0 & \delta B - 1 \end{pmatrix}. \tag{10}$$

The solution of problem (9) gives the dispersion relations which provide information about the stability of the stationary homogeneous solution (B_*, W_*, T_*) (see Cartenì *et al.* 2012). In fact, the growth rate of a perturbation characterized by a wave number h is given by the largest real part of the eigenvalues $\lambda = \lambda(h)$.

Case a): $\delta \neq 0$

When we estimate the eigenvalues of the Jacobian matrix $J(h)$ at the steady-states we obtain:

i) when $\lambda > 0$, at (B_1, W_1, T_1) the Jacobian matrix admits the eigenvalues

$$\lambda_1 = -1, \quad \lambda_2 = -\alpha - h^2\vartheta, \quad \lambda_3 = -\lambda$$

which are all negative if $\alpha > 0$. Then, the bare soil equilibrium (B_1, W_1, T_1) is stable to heterogeneous perturbations if and only if $\alpha > 0$;

ii) as we said in Section 2.1 for the homogeneous perturbations case, our analysis is performed fixing toxicity decay rate with two different values $k=0.01$ and $k=0.2$ and examining the stability character of the equilibria only depending on the parameter p. Numerical analysis, performed with the software Mathematica®, allow us to obtain that in both cases the asymptotically stable equilibria $((B_1, W_1, T_1)$ and $(B_3, W_3, T_3)^+)$ preserve their stability character. In particular, (B_1, W_1, T_1) is asymptotically stable for every value of p, and $(B_3, W_3, T_3)^+$ is still asymptotically stable for every value of $p \geq p^*(k)$, where $p^*(k) = 0.692478$, for $k=0.01$ and 0.596614 for $k=0.2$ (see Eq. (7)).

We remark that in both cases, Turing pattern conditions are not satisfied. The bifurcation diagrams related to biomass equilibria stability versus the precipitation rate p are reported in Figure 3.2a-b.

Case b): $\delta = 0$

Analogous results are obtained assuming that biomass and toxicity dynamics are decoupled. In particular, if $p \geq \dfrac{1}{2}\sqrt{\dfrac{7}{5}}$. we obtain the bifurcation diagram in Figure 3.2c.

3.3 Numerical simulations

We analyze model behaviour along an environmental gradient considering the combined effects of water availability, represented by precipitation rate p, and the persistence of toxicity in soil, represented by parameter k, that depends on the temperature,. Furthermore, we test the model behaviour with and without the effects of plant-soil negative. It has to be noted that in the latter case ($s=0$), the toxicity equation is decoupled from biomass and water

equations, and the system is equivalent to the model proposed by Klausmeier (1999) when the soil topographic variations are neglected.

All simulations were performed using zero-flux Neumann boundary conditions on a square lattice of 100x100 units, and with initial biomass peaks set as 0.2, randomly distributed over the lattice. Any simulation is carried out for 100,000 time steps, and the parameter values are summarized in Table 3.1. In addition, we also test the effects of both biomass initial condition (*IB*) and precipitation (*p*) on the emergence of spatial patterns.

Figure 3.3 shows the spatial distributions of plant biomass at the end of each simulation according to different values of precipitation rate *p* (columns), decay rate of toxicity *k* (rows), and plant sensitivity to toxic compounds *s*. In the first row (*s=0*) the simulations reproduce the typical stable spatial patterns reported in the literature for arid and semi-arid environments (Rietkerk *et al*. 2002; Gilad *et al*. 2007; Meron *et al*. 2007; Kéfi *et al*. 2010). In this case, as the precipitation rate increases, the spatial distribution of plant biomass goes from bare soil to homogeneous cover, passing through spot, labyrinth and gap patterns. Analogously, also with the effect of NF (*s=0.2*) and sufficiently high values of toxicity decay rate (*k=0.2*, Fig. 3.3 second row), the same stable patterns described above occur. In this case the toxicity is degraded too fast to affect the pattern formation, and the only visible effect is a shift of the gap pattern that occurs at higher values of precipitation. However, a significant reduction of the decay rate (*k=0.01*, Fig. 3.3 third row), produces a longer persistence of toxicity in the soil causing increased effects on the plant biomass. Moreover, for *k=0.01* and for precipitation values between 0.6 and 1.1, no stable patterns occur. In fact, distinct spots or stripes of plants are still formed, but they constantly move in time, *"escaping from the toxicity"* that accumulates in the soil patches previously occupied by the vegetation (see Supplementary Material, SPOT_k=0.01_p=0.6.avi).

This particular behaviour is clearly shown in Figure 3.4 (last row) where each panel contains a plot of the plant biomass value (*y*-axis) of the central pixel (black line) and the average value of the entire lattice (gray line) during the simulation time (*x*-axis). It is evident that for *k=0.01* and $0.6 \leq p \leq 1.1$, the biomass B_{cp} in the central point of the spatial domain, continues to oscillate indefinitely, meaning that the spots or stripes structures continue to move without reaching a stable spatial configuration (see videos in the Supplementary Material). In the other cases, the values of the biomass B_{cp} tend to be stable in time after more or less pronounced oscillations. It has also to be noted that for bare soil and uniform vegetation (i.e., no spatial pattern) the biomass value B_{cp} coincides with the average values of the lattice at the end of the simulations.

Figure 3.5 shows the effects of the initial value of biomass *IB*, the precipitation *p* and the decomposition rate *k*, on the emergence of spatial patterns. Every simulation was launched on varying *IB* within the interval [400,1600] (in all other simulations we set *IB=1000*). As shown in Figure 3.5a (*k=0.2*), bare soil emerges for *p=0.4* independently from *IB* values, and the same result is obtained for *p=0.6* and *IB<800*. In addition, with high toxicity (*k=0.01*) bare soil is obtained also for *p=0.8* and *IB<600*. On the other hand, uniform vegetation is obtained for $p \geq 1.4$ (*k=0.2*), independently of *IB*, while in case of *k=0.01*, is obtained also for *p=1.2*. Vegetation patterns emerge for all other combinations of parameters.
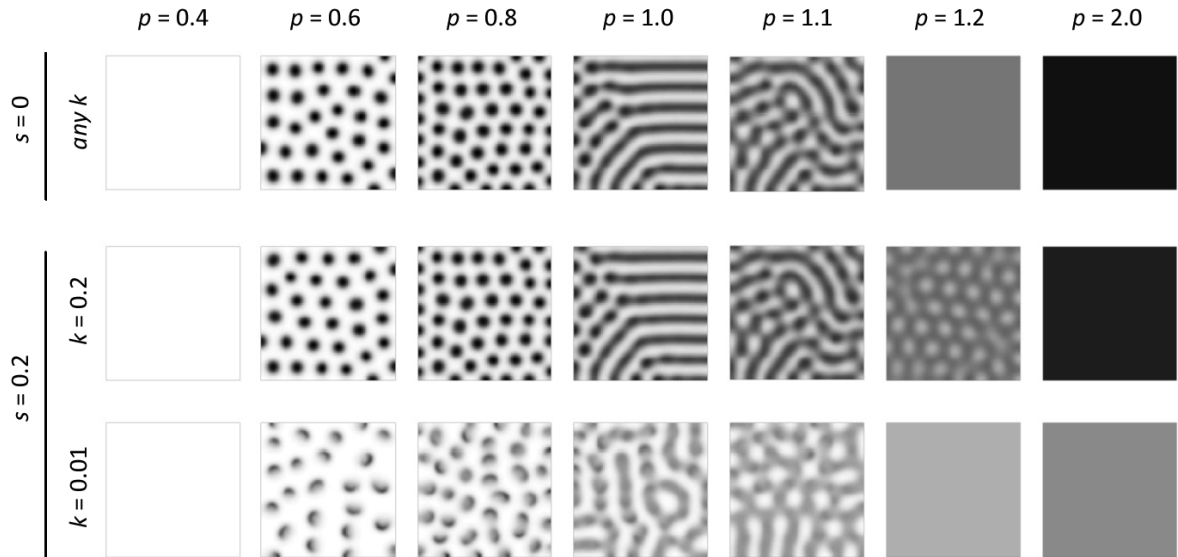
Figure 3.3. Spatial patterns emerging at different levels of precipitation p (columns), toxicity decay rate k (rows) and plant sensitivity to toxic compounds s, obtained by numerical integration of the model equations Eq. (1). Each panel shows a grey-scale map of biomass distribution with darker shade representing higher biomass density. In the first row ($s=0$) the model behaves independently of toxicity T, reproducing the typical spatial patterns reported for arid and semi-arid environments. Analogous results are produced with the effect of NF ($s=0.2$) and high values of toxicity decay rate ($k=0.2$, second row). On the other hand, a significant reduction of the decay rate ($k=0.01$, third row) still produces distinct spots or stripes of plants, but they constantly move in time, escaping from the toxicity that accumulates in the previously occupied soil patches. Other parameter values are reported in Table 3.1.
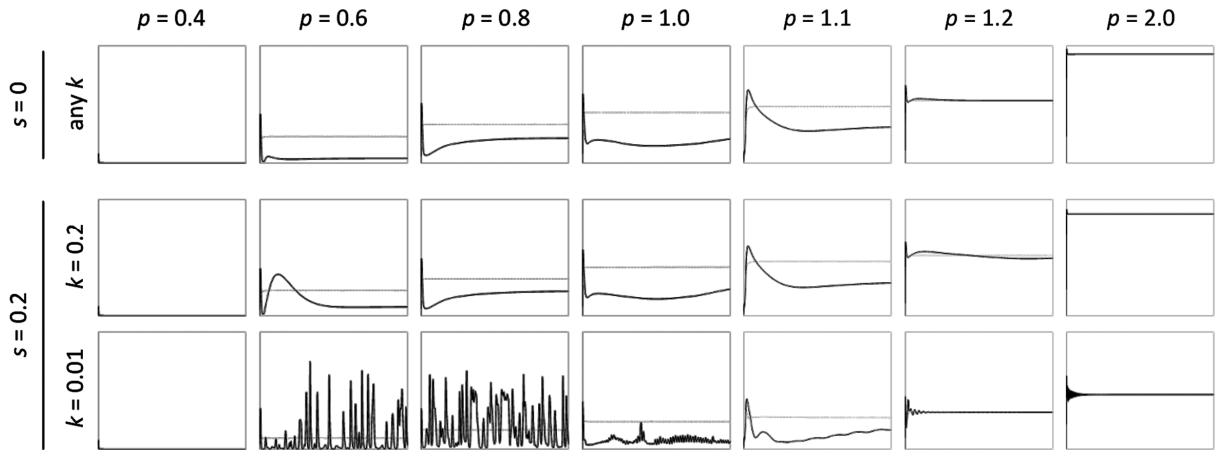
Figure 3.4. Plots of the biomass value B_{cp} in time (x-axis) of the central pixel of the simulation domain (black line) compared to the average value of the entire lattice (gray line), at different levels of precipitation p (columns), toxicity decay rate k (rows) and plant sensitivity to toxic compounds s. Biomass values B_{cp} tend to be stable in time after more o less pronounced oscillations. It has to be noted that for $k=0.01$ and $0.6 \leq p \leq 1.1$, the biomass in the central point continues to oscillate indefinitely in time, meaning that the spots or stripes structures continue to move without reaching a stationary spatial configuration. Other parameter values are reported in Table 3.1.
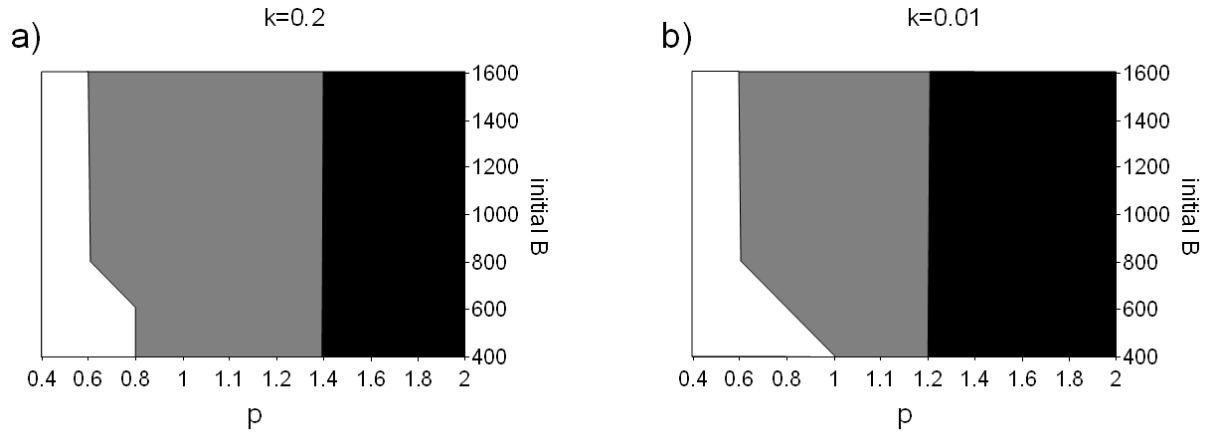
Figure 3.5. Effects of precipitation *p*, initial biomass *IB,* and decomposition rate *k* on pattern formation. The two panels (panel a: *k*=0.2; panel *b*: *k*=0.01) show the emerging spatial pattern as a function of precipitation rate (0.4≤ *p* ≤2.0) and the initial value of the biomass *B*. White, grey, and black zones correspond to bare soil, vegetation pattern (i.e. spot, labyrinth or gaps), and homogeneous vegetation, respectively.

4. Discussion and research perspectives

Owing to the analytical difficulties to study mathematical models consisting of more than two equations, the *quasi-steady-state approach* is often employed to perform a stability analysis and to verify Turing conditions. This method is based on the phenomenological assumption that the dynamics of one state variable are much faster than the others. In vegetation pattern models with soil and surface water, the last one is often assumed to be constant, then the model is reduced to only two PDEs (HillerisLambers *et al*. 2001; Kéfi *et al*. 2010). However, this approach presents some drawbacks as shown by Flach and Schnell (2006), then we have chosen to avoid this kind of assumption, although the analysis of our model presents a huge mathematical complexity as in (Sherratt 2005, 2010; Sherratt and Lord 2007).

We showed that the mechanism underlying pattern formation, even though Turing conditions are not satisfied, originates from the contribution of both positive and negative feedbacks. In detail, depending on environmental conditions, our model exhibits a bistability area (Fig. 3.2) (von Hardenberg *et al*. 2001; Rietkerk *et al*. 2002), i.e., the coexistence of two stable and one unstable states for the same values of parameter *p*. Moreover, when the high presence of toxicity in the soil makes the NF overwhelming with respect to positive water feedback, a phenomenon of dynamical stabilization occurs (Petrovskii *et al*. 2001). In this case, our vegetation system evolves to spatial patterns that are spatially unstable in time. Due to the nonlinear contribution of both feedbacks, our model exhibits the presence of vegetation patterns in an area of the parameters space *p-k* where the bare soil is the only existing homogeneous equilibrium and it is also stable both for the spatial and nonspatial perturbations (Fig. 3.2). Nevertheless, as in (Rietkerk *et al*. 2002; Meron *et al*. 2004, 2007; Kéfi *et al*. 2010; Meron 2010), when the rainfall decreases, the vegetation cover shifts from uniform to gaps, labyrinths, spots and, finally, bare soil. It has to be noted that with high toxicity persistence in soil (Fig. 3.5b, *k*=0.01), regular vegetation patterns occur in a smaller region of the parameter space compared to lower or absent persistence (Fig. 3.5a, *k*=0.2). This can be explained remembering that toxicity is a factor that enhances plant mortality. In the presence of low precipitation, a bigger amount of initial biomass is needed to prevent bare soil, while for

higher precipitation rates, toxicity has a destabilizing effect that breaks the pattern formation leading to homogeneous vegetation covers.

In our model, opposing forces interact to create the peculiar observed biomass dynamics. In fact, on the one hand, the low water availability promotes the aggregation of biomass into isolated spots or stripes due to the local facilitation properties of the system. On the other hand, the aggregation of biomass produces local high levels of toxicity forcing the plants to propagate where the negative effect of T in the soil is lower. An interesting result, when the discussed interacting forces are not balanced, is the occurrence of patterns that continuously move in space. This phenomenon becomes more evident as the persistence of toxicity in the soil increases, i.e., as parameter k decreases. In particular, for low values of toxicity decay and precipitation rates, the vegetation spots constantly move in the space due to the accumulation of toxicity in the soil (SPOT_k=0.01_p=0.6.avi in Supplementary Material). Moreover, also for higher precipitation rates ($p{\geq}0.6$), i.e., when the vegetation pattern shape reaches a stationary configuration, the biomass continuously move within the patches (see LABYRINTH_k=0.01_p=1.0.avi and GAP_k=0.01_p=1.1.avi in Supplementary Material).

In addition, the typical shape of spots and stripes is not neat and symmetrical as the ones observed in other model simulations (Rietkerk *et al*. 2002; Meron *et al*. 2004, 2007; Gilad *et al*. 2007; Kéfi *et al*. 2010; Meron 2010). Indeed, in our simulations, each spot has the biomass peak shifted towards the side it is moving to, and not in its centre (as in the usual simulated patterns) since this is the zone with the highest toxicity accumulation. Further simulations were performed to study the asymmetrical patterns. As we show in Figure 3.6, the overall shape of the spot changes according to the persistence of toxicity in the soil (parameter k). In detail, analyzing the biomass distribution along a central transect, we clearly show the different shapes of the spots in absence of toxic effects (Fig. 3.6, left panel) and with increasing toxicity (Fig. 3.6, right panel). In the first case, the spot presents the usual symmetrical shape as predicted by other model simulations. In the second case, the effect of the spots movement is made evident by the shift of the peak towards the direction corresponding to a less concentration of toxicity (direction of biomass movement is indicated by the arrow in Fig. 3.6, right panel). Moreover, the biomass distribution presents a tail on the side opposite to the movement direction. The shape of such biomass tail is found to be highly dependent on the persistence of toxicity in the soil. Specifically, with low values of k (k=0.005 in Fig. 3.6, right panel), the biomass tail is almost absent due to the high toxicity left in the previously occupied soil. On the contrary, with higher k values (k=0.01 and k=0.015, in Fig. 3.6, right panel), the toxic effect decreases allowing a higher portion of biomass to persist in the tail. This effect clearly creates the asymmetric vegetation patterns.

From an ecological point of view, both the continuous movement and the asymmetrical shape of the patterns are very relevant phenomena, although its time scale (years) makes them difficult to be observed and studied with field experiments. Analysis of aerial photographs was carried out, and shown in Figure 3.7, to test the asymmetrical patterns behaviour in two sites reported in literature (Deblauwe *et al*. 2008). Using specific filters, the aerial photographs (Fig. 3.7 first column) have been edited to highlight zones of high (black), medium (dark grey) and low (light grey) biomass density (Fig. 3.7 second column), and then are compared to model simulations (Fig. 3.7 third column). Such analysis clearly shows a good qualitative correspondence between real vegetation spots and the ones predicted by model simulations (Fig. 3.7 first row). Similarly, labyrinths present an heterogeneous distribution of biomass within the stripes that was also observed in natural patterns (Fig. 3.7 second row).
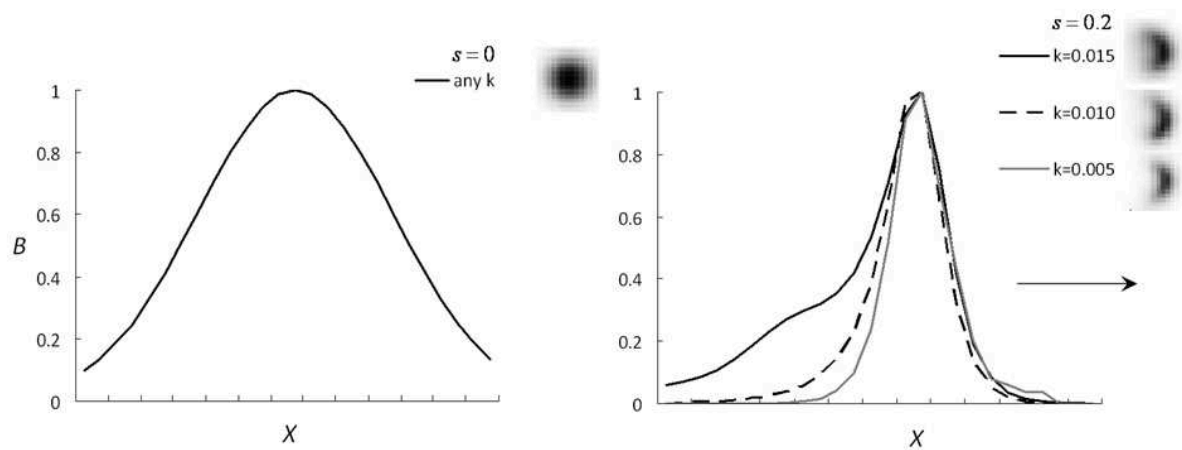
Figure 3.6. Transect view of single biomass spots at different levels of plant sensitivity to toxic compounds (s) and toxicity decay rate (k). Each panel shows the concentration of plant biomass B along a single spatial dimension (x) at the end of a simulation run. In the left panel, the model is only influenced by biomass-water dynamics and the simulation produces stable isolated spots with typical distribution of biomass with a peak in the centre. The right panel shows the shape of the biomass curve in response to three levels of k, in the case of simulated spots that continuously moving in space. The arrow indicates the direction of the moving biomass front. The top-right corner of each panel shows the positioning of the plane view of simulated spots.

| Real photo | Photo-interpretation | Simulation |
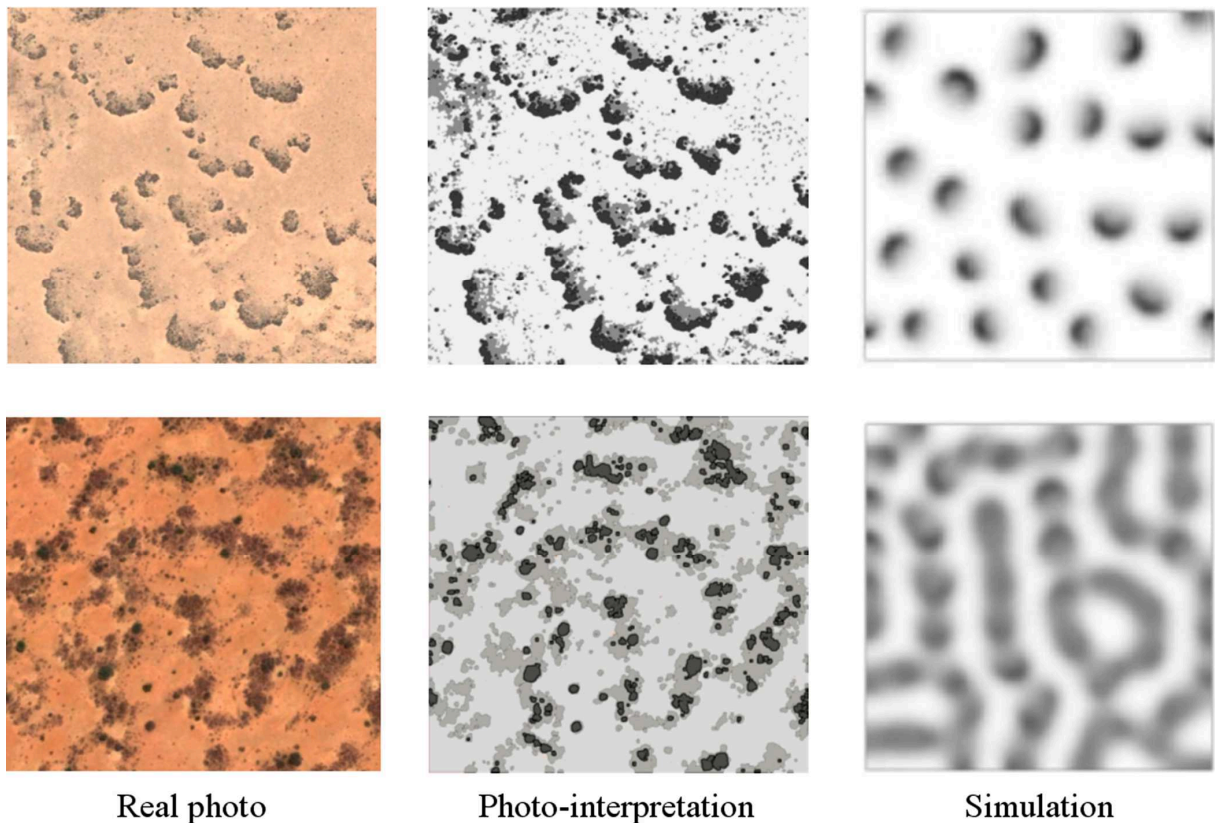
Figure 3.7. Comparison of model simulation outputs (spots and labyrinths in rows) with aerial photographs of real vegetation patterns and image interpretation. Spots and labyrinths refer to California, 26°48' N, 112°53' O and Sudan, 11°08' N, 27°50' E, respectively.

38

Acknowledgements

Supplementary material

Supplementary videos (SPOT_k=0.01_p=0.6.avi; LABYRINTH_k=0.01_p=1.0.avi; GAP_k=0.01_p=1.1.avi) can be found at the following web page:

http://wpage.unina.it/giannino/video/

4

MODELLING THE DEVELOPMENT AND ARRANGEMENT

OF PRIMARY VASCULAR STRUCTURE IN PLANTS

―――――――――――――――――――――

Fabrizio Cartenì, Francesco Giannino, Fritz Hans Schweingruber and Stefano Mazzoleni.
In press on Annals of Botany

Abstract

• *Background and Aims* The process of vascular development in plants results in the formation of a specific array of bundles that run throughout the plant in a characteristic spatial arrangement. Although much is known about the genes involved in the specification of procambium, phloem and xylem, the dynamic processes and interactions that define the development of the radial arrangement of such tissues remain elusive.

• *Methods* In this study we present a spatially explicit reaction-diffusion model defining a set of logical and functional rules to simulate the differentiation of procambium, phloem and xylem and their spatial patterns, starting from an homogeneous group of undifferentiated cells.

• *Key Results* Simulation results showed that the model is capable of reproducing most vascular patterns observed in plants, from primitive and simple structures constituted of a single strand of vascular bundles (protostele), to more complex and evolved ones, with separated vascular bundles arranged in an ordered pattern within the plant section (e.g. eustele).

• *Conclusions* Presented results demonstrated, as a proof of concept, that a common genetic-molecular machinery can be at the base of different spatial patterns of plant vascular development. Moreover, the model could become a useful tool to test different hypotheses of genetic and molecular interactions involved in the specification of vascular tissues.

Introduction

During growth of plant axial organs, the process of vascular development takes place in two specific regions located right below the shoot and root apical meristems. Such developmental processes result in the formation of a specific array of vascular bundles that run throughout the plant in a characteristic spatial arrangement. One of the first events in plant development that precedes the differentiation of the provascular tissues (as well as other tissues) is the establishment of polarity with the differential expression of patterning genes along both the apical-basal and the central-peripheral axes. Considering the radial patterning alone, the juxtaposition of the central and peripheral domains is thought to drive cotyledon and leaf outgrowth (Waites *et al*. 1998) as well as providing a direct input in the radial patterning of vascular bundles (Carlsbecker and Helariutta 2005).

Two distinct levels of spatial organization can be distinguished within the vascular system (Esau 1977): a longitudinal pattern, i.e. the array of vascular bundles within an organ; and a radial pattern which is the spatial arrangement of phloem and xylem within each vascular bundle and, more generally, within a transversal plant section. For the scope of our work we will concentrate our attention on the radial pattern of plant stems and roots. In such context, new procambium, phloem and xylem are consistently differentiated in a specific spatial pattern that varies between organs and species. The combination of the vascular tissues of stems and roots with any other associated fundamental or ground tissue, such as pith and interfascicular regions, is defined "stele" or "central cylinder" (Esau 1977). Beck *et al.* (1982) listed several types of recognized steles and classified them into three basic types: i) protostele presenting a solid column of vascular tissue; ii) siphonostele characterised by an hollow cylinder of vascular tissue; iii) eustele showing separated strands of vascular tissue, usually arranged as a discontinuous cylinder.

Much attention has been given to hormonal (Bowman and Floyd 2008; Vanstraelen and Benková 2012) and genetic (Caño-Delgado *et al*. 2010) control of developmental events and in particular to the role of auxin polar transport in the patterning of developing organs (Blilou *et al*. 2005; Teale *et al*. 2006), somehow ignoring the stimuli responsible for its involvement. Recent works on *Arabidopsis* roots provided new insights on the mechanisms controlling vascular patterning. Bishopp *et al*. (Bishopp, Help, *et al*. 2011; Bishopp, Lehesranta, *et al*. 2011) investigated the roles of auxin and cytokinin in specifying and maintaining the radial patterning of xylem cells, identifying the feedback loop network between hormonal signalling and transport. On the other hand, phloem is established through asymmetric cell divisions followed by differentiation. APL, a myb family transcription factor, has been identified to promote such developmental events (Bonke *et al*. 2003). In *apl* mutants, xylem differentiates in place of phloem cells and, interestingly, when *APL* is ectopically expressed, the differentiation of xylem precursors is suppressed. Evidence from studies on *Arabidopsis* mutants (Kerstetter *et al*. 2001; Eshed *et al*. 2001) shows that ectopic expression of *KANADI* genes results in abaxialized organs that do not develop any vasculature. These results suggested the antagonistic role of *HD-ZIP III* and *KANADI* genes and that the establishment of both adaxial/central and abaxial/peripheral domains is needed for the correct development of vascular tissues (Ilegems *et al*. 2010).

In the late 70's, Wilson (1978) proposed an hypothesis, based on experimental evidence, for the differentiation of vascular tissues in regenerating cambia involving opposing gradients of auxin and sucrose. Recently, new studies highlighted the possible interplay between sugar and auxin in plant growth and development (reviewed in Eveland and Jackson 2011). Searching for genes expressed during the first stages of leaf development, Pien *et al.* (2001) found five genes showing a specific spatial pattern of expression within apical meristems. Interestingly, three of those genes encoded enzymes involved in sugar metabolism, showing evidence that also carbohydrate metabolism is spatially regulated during key developmental processes.

In the last decades, simulation models have proven to be useful tools to unravel the often non-intuitive relations between local processes and the emergence of global forms and patterns (Jönsson and Krupinski 2010). Several studies using computational modelling have been carried out on plant morphodynamics (reviewed in Prusinkiewicz and Runions 2012) and recent work (reviewed in Jönsson *et al*. 2012) has focused on two topics: i) venation and phyllotaxis driven by auxin polar transport and ii) genetic regulation of stem cells in apical meristems (Fujita *et al*. 2011). In particular, modelling studies on vascular development mainly concentrated on the role of auxin in leaf venation. The first model was formulated by Sachs (1969) proposing the so called "canalization hypothesis". According to this model, auxin export through a cell wall promotes further transport in the same direction, thus creating canals of preferential flow as a self-organization property of the system. Based on this hypothesis, many molecular models were formulated (e.g. Mitchison 1980; Feugier *et al*. 2005; Bayer *et al*. 2009) and tested against experimental data (e.g. Scarpella *et al*. 2006). A recently published work (Muraro *et al*. 2013) based on the work of Bishopp *et al*. (2011) presents a simulation model providing useful insights on the signalling network behind the radial patterning of procambium and xylem in *Arabidopsis* root.

Aside from the work of Muraro *et al*. (2013), no modeling effort has been done yet to study the radial patterning of primary vascular structures, i.e., the specification and spatial organization of procambium, phloem and xylem. Moreover, as far as we know, there are no published models able to simulate the diversity of steles observed in nature. In this study we present a spatially explicit reaction-diffusion model inspired by the pioneering works of Turing (1952) and Meinhardt (1982). Our model defines a set of logical and functional rules able to simulate the differentiation of procambium, phloem and xylem and the emerging radial patterns of vascular tissues. The model qualitatively reproduces most stelar structures observed in different plant taxa, demonstrating, as a proof of concept, that a common genetic-molecular machinery can be at the base of vascular development and patterning.

Methods

Model description

We assume that a concentration gradient of a morphogenetic factor is established within plant meristems that is interpreted by cells as a positional cue to initiate the definition of the central and peripheral domains. The following differentiation of vascular cells, strictly depends on the establishment of the radial patterning. In particular, the juxtaposition of central and peripheral domains is assumed to be indispensible for procambium definition and to provide positional cues for the specification of phloem and xylem. Scattered evidence is available on the spatial processes involved in the specification of procambium. Auxin seems to regulate the initiation of procambial cells during early embryo development. In the absence of auxin signalling mediated by MONOPTEROS (MP), an auxin-responsive factor, procambial cells do not form properly (Hardtke and Berleth 1998). Wilson (1978) proposed the hypothesis that two morphogens, centrifugally diffusing auxin and centripetally diffusing sucrose, were responsible for the positioning of regenerating cambium after wounding. Based on these evidence, we assume that the activation of genes involved in procambium differentiation require the presence of two different substances with opposing gradients. Moreover, phloem and xylem tissues are always found associated to one another and arranged in consistent patterns within each organ. It is possible to assume that the genes and molecules responsible for their differentiation somehow inhibit each other locally (meaning that a single cell can only become either phloem or xylem), but also facilitate each other laterally so that both tissues can differentiate at the same time. These assumptions are supported by the antagonistic role of HD-ZIP IIIs and KANADIs in the determination of the adaxial-abaxial

organ polarity and the regulation of vascular tissues specification (Emery *et al*. 2003) and also by the evidence on the effects of APL on phloem and xylem differentiation (Bonke *et al*. 2003). For the sake of simplicity, we used reaction-diffusion formulations that could adequately mimic the general behaviour of the abovementioned interactions.

Based on such premises, we implemented a mathematical model that simulates the development of a group of undifferentiated cells in a sub-apical transverse section of stems and roots (Fig. 4.1). The model is composed of 3 groups of partial differential equations (PDEs), each module describing a set of developmental events leading to the differentiation of vascular tissues.
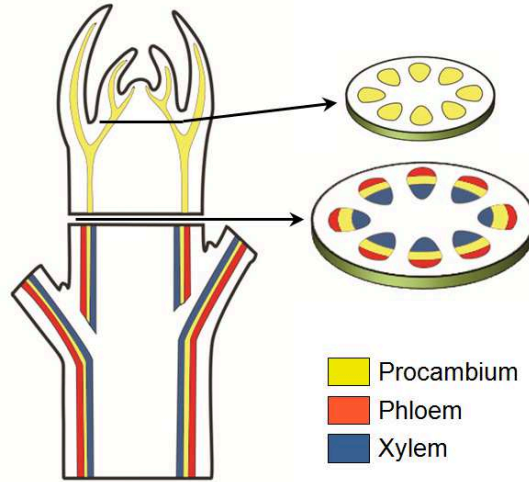
Figure 4.1. Schematic representation of a typical arrangement of vascular tissues in plants.

Spatial domain definition. The first equation describes the dynamics of the first morphogenetic factor, S_0 within each cell. Its production is assumed to be a linear function of the distance from the centre of the section (d), while its consumption is due to a constant rate μ_{S0}. So, we can write:

$$\frac{\partial S_0}{\partial t} = \sigma_{S0}\left(\frac{d}{r}\right) - \mu_{S0}S_0 + D_{S0}\Delta S_0 \tag{1}$$

where σ_{S0} is the basic production rate, r is the radius of the domain and D_{S0} is the diffusion coefficient. Cells that have an S_0 concentration lower than a threshold value (S_0^*) trigger the production of a specific diffusible signal S_1, while concentrations that are higher or equal to S_0^* trigger the production of another specific diffusible signal S_2 (Fig. 4.2A).

Procambium. The differentiation of procambium is formulated as an activator-substrate system (Meinhardt 1982) describing the dynamics of two diffusible substrates and one diffusible autocatalytic activator. Signals S_1 and S_2 have the role of substrates and they are both consumed to promote the autocatalytic reaction of the procambium activator A_P (Fig. 4.2B). The system is written as:

$$\frac{\partial S_1}{\partial t} = \overline{\sigma_{S1}}\left(1 - \frac{S_1}{1+k_S A_P}\right) - \rho_S A_P^2 S_1 S_2 + D_S \Delta S_1 \tag{2}$$

$$\frac{\partial S_2}{\partial t} = \overline{\sigma_{S2}}\left(1 - \frac{S_2}{1+k_S A_P}\right) - \rho_S A_P^2 S_1 S_2 + D_S \Delta S_2 \tag{3}$$

$$\frac{\partial A_P}{\partial t} = \sigma_{AP} + \rho_{AP} A_P^2 S_1 S_2 - \mu_{AP} A_P + D_{AP}\Delta A_P \tag{4}$$

where $\overline{\sigma_{S1}}$ and $\overline{\sigma_{S2}}$ are spatially variable parameters defined as follows:

$$\overline{\sigma_{S1}} = \begin{cases} \sigma_S, & S_0 < S_0^* \\ 0, & S_0 \geq S_0^* \end{cases}$$

$$\overline{\sigma_{S2}} = \begin{cases} 0, & S_0 < S_0^* \\ \sigma_S, & S_0 \geq S_0^* \end{cases}$$

and σ_S is the basic production rate of the two substrates that are specifically produced in different conditions: S_1 is produced only in the central domain ($S_0 < S_0^*$) while S_2 only in the peripheral domain ($S_0 \geq S_0^*$); σ_{AP} is the basic production rate of the procambium activator; k_S is the saturation constant of substrates production; ρ_S and ρ_{AP} are the cross-reaction coefficients; μ_{AP} is the removal rate of A_P and D_S and D_{AP} are the diffusion coefficient. If the concentration of A_P is higher or equal than the threshold value A_P^*, triggers the differentiation of procambium (Fig. 4.2C).

Phloem and xylem. The differentiation of phloem and xylem vascular tissues is described by the dynamics of two autocatalytic activators (A_F and A_X, promoting the differentiation of phloem and xylem respectively) that exclude each other locally through the production of a common repressor R, but mutually activate each other over long range via the production of each other's substrate (S_F and S_X). Moreover, facilitation of phloem in the peripheral zone and xylem in the central zone are considered (Fig. 4.2D). The equations are formulated, based on Meinhardt and Gierer (1980), as follows:

$$\frac{\partial A_F}{\partial t} = \overline{Pro}\left(\sigma_{AXF} + \rho_{AXF}\frac{A_F^2 S_F}{1+R}\right) - \mu_{AXF}A_F + D_{AF}\Delta A_F \tag{5}$$

$$\frac{\partial A_X}{\partial t} = \overline{Pro}\left(\sigma_{AXF} + \rho_{AXF}\frac{A_X^2 S_X}{1+R}\right) - \mu_{AXF}A_X + D_{AX}\Delta A_X \tag{6}$$

$$\frac{\partial S_F}{\partial t} = \overline{Pro}\left(\overline{\sigma_{SF}} + \gamma_{SXF}(A_X - S_F)\right) - \mu_{SXF}S_F + D_{SXF}\Delta S_F \tag{7}$$

$$\frac{\partial S_X}{\partial t} = \overline{Pro}\left(\overline{\sigma_{SX}} + \gamma_{SXF}(A_F - S_X)\right) - \mu_{SXF}S_X + D_{SXF}\Delta S_X \tag{8}$$

$$\frac{dR}{dt} = \rho_{AXF}A_F^2 S_F + \rho_{AXF}A_X^2 S_X - \mu_R R \tag{9}$$

where $\overline{PRO}$ is a spatially variable parameter defined as:

$$\overline{PRO} = \begin{cases} 0, & A_P < A_P^* \\ 1, & A_P \geq A_P^* \end{cases}$$

meaning that the substances in equations (5-9) are only produced and react within differentiated procambial cells ($A_P \geq A_P^*$). Two more spatially variable parameters, $\overline{\sigma_{SF}}$ and $\overline{\sigma_{SX}}$, are included to define the local facilitation of phloem and xylem activation. Here we assume the promotion of phloem over the peripheral zone and the xylem over the central zone, defined as follows:

$$\overline{\sigma_{SF}} = \begin{cases} 0, & S_0 < S_0^* \\ \sigma_{SXF}, & S_0 \geq S_0^* \end{cases}$$

$$\overline{\sigma_{SX}} = \begin{cases} \sigma_{SXF}, & S_0 < S_0^* \\ 0, & S_0 \geq S_0^* \end{cases}$$

σ_{AXF} and σ_{SXF} are the basic production rates, ρ_{AXF} and γ_{SXF} are the reaction coefficients, μ_{AXF}, μ_{SXF} and μ_R are the removal rates, and D_{AF}, D_{AX} and D_{SXF} are the diffusion coefficients. If the concentration of either A_F or A_X is higher or equal than the threshold value A^*, triggers the differentiation into phloem or xylem, respectively (Fig. 4.2E).

Figure 4.2 graphically explains the general behaviour of all three parts of the model. Moreover, Figure 4.3 shows the diagram of the model steps leading to the differentiation of vascular tissues from the point of view of a single cell.
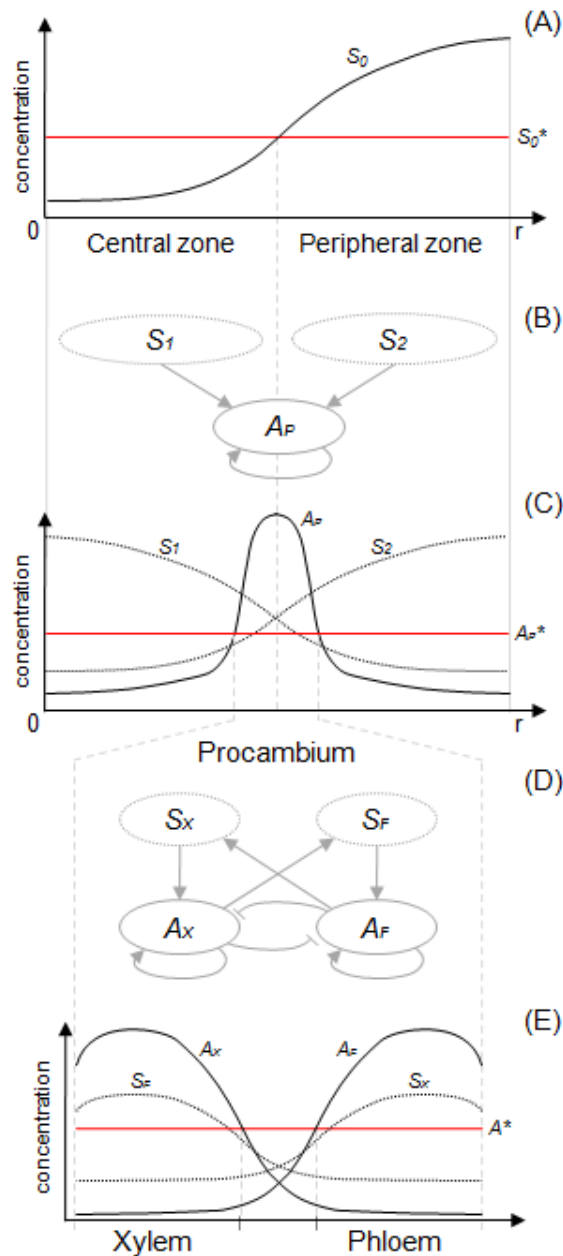
Figure 4.2. Schematic representation of model processes. A) Steady state profile of S_0 concentration along the section radius. Central and peripheral zones are defined according to S_0^*. B) Procambium substrates-activator dynamics described by eqns (2)-(4). C) Steady state profile of S_1, S_2 and A_P along the radius of a simulated plant section. A_P peak is established at the boundary between the central and peripheral zones as an emergent property of both S_1 and S_2 concentration gradients. Procambium is differentiated where A_P is above the threshold value A_P^*. D) Xylem and phloem activators dynamics described by eqns (5)-(9). E) Steady state profile of xylem and phloem activators (A_X and A_F) and substrates (S_X and S_F) within a procambial strand.
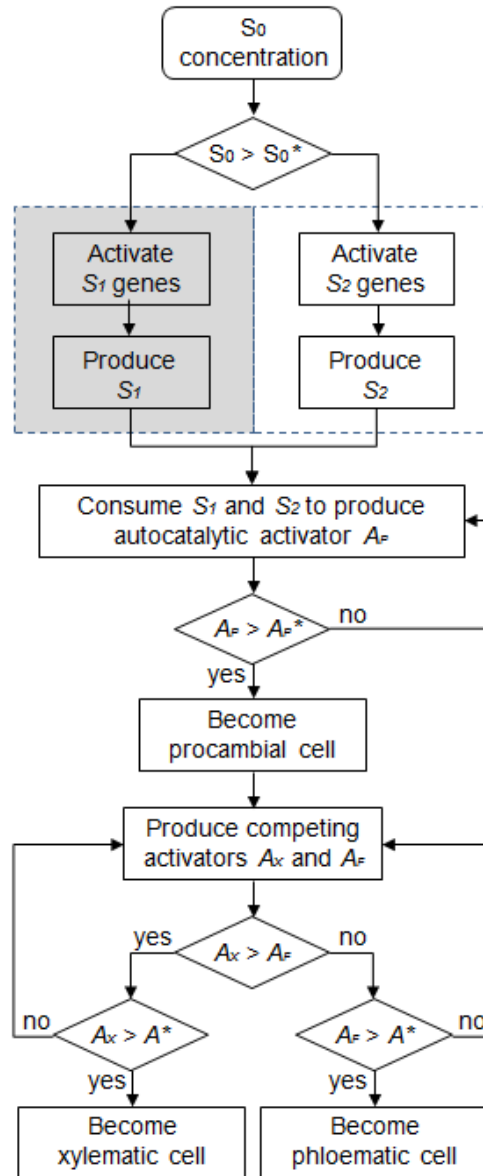
Figure 4.3. Diagram of the model steps leading to the differentiation of vascular tissues from the point of view of a single cell.

Numerical simulations

All numerical calculations were implemented in MATLAB R2012b (MathWorks Inc.) and the reaction-diffusion dynamics were integrated using Euler method. The simulations were carried out for a total time $T = 20000$ (and a time step $dt = 0.1$) or until steady state was reached. The plant section, i.e. the equations spatial domain, was set as a circular lattice with zero-flux Neumann boundary conditions and radius r (number of pixels). The initial value of all state variables was set to zero. Tables 4.1 and 4.2 contain the list of all parameters and the values used in numerical simulations. For simplicity, no domain growth was considered during the simulations.

The model analysis has been performed through a series of numerical simulations:

i) The definition of central and peripheral zones has been tested in relation to section radius r;

ii) The emergence of procambial spatial patterns has been assessed in relation to the change of two parameters: section radius r and procambium cross-reaction coefficient ρ_{AP}.

47

iii) Starting from different arrangements of procambium, the effects of A_F and A_X diffusion coefficients (D_{AF} and D_{AX}) on the emergent patterns of phloem and xylem were tested.

A qualitative comparison between simulated patterns and observed vascular arrangements (as classified by Beck *et al*. 1980) was carried out.

Table 4.1. List of equations (1-4) parameters and simulation values

Parameter	Description	Value
σ_{S0}	S_0 basic production rate	0.012
r	radius of the domain	20; 40
d	distance from centre of the domain	[0 r]
μ_{S0}	S_0 consumption rate	0.015
D_{S0}	S_0 diffusion coefficient	0.8
σ_S	S basic production rate	0.04
k_S	S production saturation constant	20
ρ_S	S cross-reaction coefficient	0.08
D_S	S diffusion coefficient	0.5
σ_{AP}	A_P basic production rate	0.001
ρ_{AP}	A_P cross-reaction coefficient	0.03; 0.05
μ_{AP}	A_P removal rate	0.02
D_{AP}	A_P diffusion coefficient	0.02
S_0*	threshold value for definition of central/peripheral zones	0.5
A_P*	threshold value for differentiation of procambium	0.5

Table 4.2. List of equations (5-9) parameters and simulation values

Parameter	Description	Value
σ_{AXF}	A_F and A_X basic production rate	0.01
ρ_{AXF}	A_F and A_X cross-reaction coefficient	0.1
μ_{AXF}	A_F and A_X removal rate	0.01
D_{AF}	A_F diffusion coefficient	0.001-0.003
D_{AX}	A_X diffusion coefficient	0.001-0.003
σ_{SXF}	S_F and S_X basic production rate	0.001
γ_{SXF}	S_F and S_X reaction coefficient	0.03
μ_{SXF}	S_F and S_X removal rate	0.01
D_{SXF}	S_F and S_X diffusion coefficient	0.02
μ_R	R removal rate	0.5
$A*$	threshold value for differentiation of phloem and xylem	30

RESULTS

Central and peripheral zones definition

The simple diffusive processes described by eqn. (1) produce a rapid change of the concentration of S_0 which reaches the steady state with a concentration gradient along the radius (Fig. 4.2A), with a maximum at the boundary of the domain and a minimum at the centre. For values of the radius $r > 10$, eqn (1) consistently produces two distinct zones, one internal with $S_0 < S_0^*$ and one external with $S_0 \geq S_0^*$, while for values of the radius $r \leq 10$, the concentration of S_0 was found to be higher than S_0^* in all the domain, thus failing to produce the internal zone (simulations not shown).

Procambium differentiation

The emergent spatial pattern of procambium differentiation was found to be highly dependent on the cross-reaction coefficient of the procambium activator (ρ_{AP}) and the radius of the simulated spatial domain (r). As shown in Figure 4.4, no procambium is differentiated for low reaction coefficients ($\rho_{AP} \leq 0.020$) as well as for very small sections ($r \leq 10$). In the first case, no peaks of A_P may establish due to the insufficient conversion of the substrates into activator, while in the second case the production of A_P cannot start due to the absence of substrate S_1 production because of the concentration gradient of S_0 (see previous section). A protostelic structure (P) consistently emerges for domains with a radius lower than 30, while, for higher radiuses, either eustelic (E) or siphonostelic (S) patterns emerge, clearly depending on parameter ρ_{AP}. The eustele and siphonostele structures differentiate for low and high values of ρ_{AP} respectively. Interestingly, for values of ρ_{AP} around 0.038 an intermediate pattern between eustele and protostele emerges (SE in Fig. 4.4), where isolated spots arranged in an eustelic pattern are still connected by a continuous thin ring of procambial cells.

The increase in the cross-reaction coefficient ρ_{AP}, resulted in a shift from a spotted to a striped pattern, which is coherent with the work on activator-substrate systems by Meinhardt (1982). The striped pattern assumes a ring shape due to the emergent property of activator peaks positioning. Activator autocatalysis needs two substrates that are produced in distinct areas. For this reason A_P peaks tend to form at the boundary between the two areas, i.e. where both substrates are most available. As the domain size decreases, spots or stripes that are usually segregated begin to form closer to one another until they merge together forming a single spot in the centre of the domain ($r \leq 30$). Such protostelic structures are typically found in roots of most plant species and also in some stems, particularly of primitive species.

Other parameters such as the diffusion coefficients (D_{AP} and D_S) were found to have no effect on the type of pattern generated, but related to other features like the width of A_P peaks, i.e. the width of procambium spots and rings (simulations not shown).
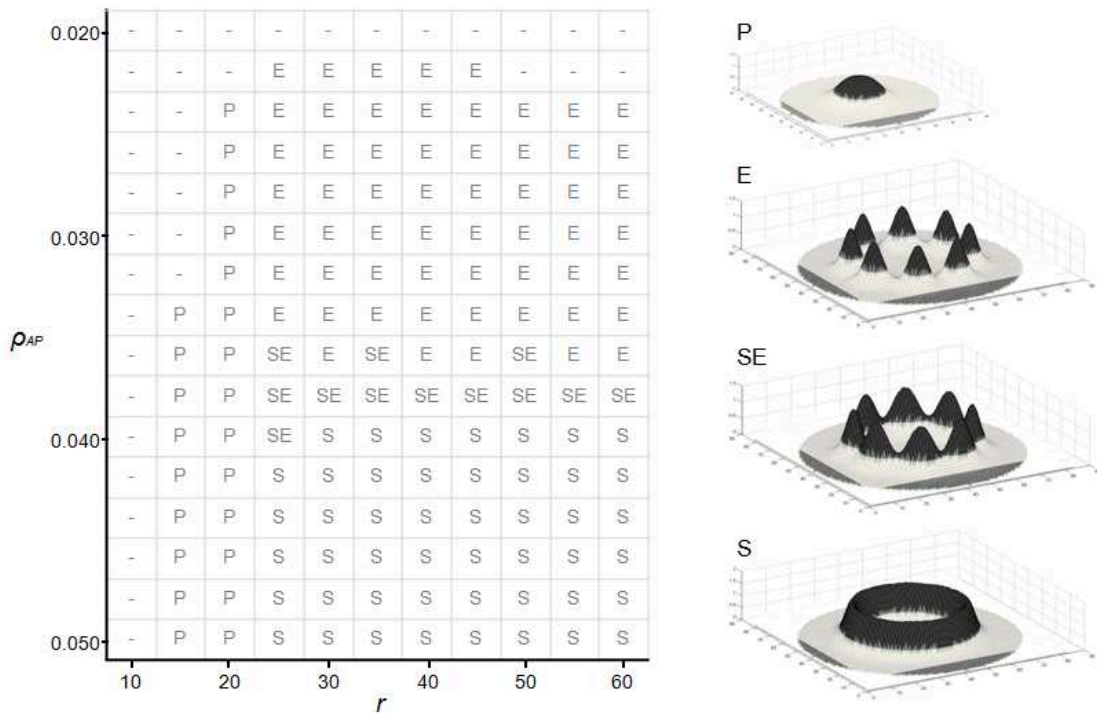
Figure 4.4. Effects of radius r and cross-reaction coefficient ρ_{AP} on procambium differentiation patterns. A protostelic structure (P) is formed for domains with a radius lower than 30, while, for higher radiuses, eustelic (E) and siphonostelic (S) patterns emerge. An intermediate pattern between siphonostele and eustele emerges (SE) for values of ρ_{AP} around 0.038. Other parameter values are listed in Table 4.1. See text for details.

Phloem and xylem differentiation

In the second simulated experiment (Fig. 4.5), we tested the effects of both the diffusion coefficients of phloem and xylem activators (D_{AX} and D_{AF}) and the starting spatial configuration of procambium (depending on ρ_{AP} and r) on phloem and xylem differentiation patterns. The diffusion coefficients were progressively increased, in a factorial combination, from 0.001 up to 0.003. In general, as the diffusion coefficients increase, so does the width of the activators peaks. According to this, with $D_{AX} = D_{AF} = 0.001$, a central band of xylem is formed surrounded by phloem both on the inside and the outside, generating three easily recognizable structures: amphiphloic protostele (Fig. 4.5, section 1); eustele with bicollateral bundles (Fig. 4.5, section 2); amphiphloic siphonostele (Fig. 4.5, section 3). With $D_{AX} = D_{AF} = 0.002$, the size of activators peaks start to increase and so does the competition for space, creating two more distinct patterns: actinostele (Fig. 4.5, section 4) with spots of phloem on the outside of the vascular strand with internal star-shaped xylem; eustele with collateral bundles (Fig. 4.5, section 5; [**Supplementary Information - Video S1**]). Similarly, for $D_{AX} = D_{AF} = 0.003$, a protostele with mixed phloem and xylem (Fig. 4.5, section 7) and an ectophloic siphonostele (Fig. 4.5, section 9; [**Supplementary Information - Video S2**]) are formed. Interestingly, for decoupled values of the diffusion coefficients ($D_{AX} \neq D_{AF}$), every single vascular bundle differentiate with one tissue type completely surrounded by the other. In particular, the one with the higher diffusion coefficient consistently occupies the central position and four new observed structures are produced by simulations: ectophloic (Fig. 4.5, section 10) and endophloic (Fig. 4.5, section 12) protostele; eustele with amphicribal (Fig. 4.5, section 11) and amphivasal (Fig. 4.5, section 13) bundles.
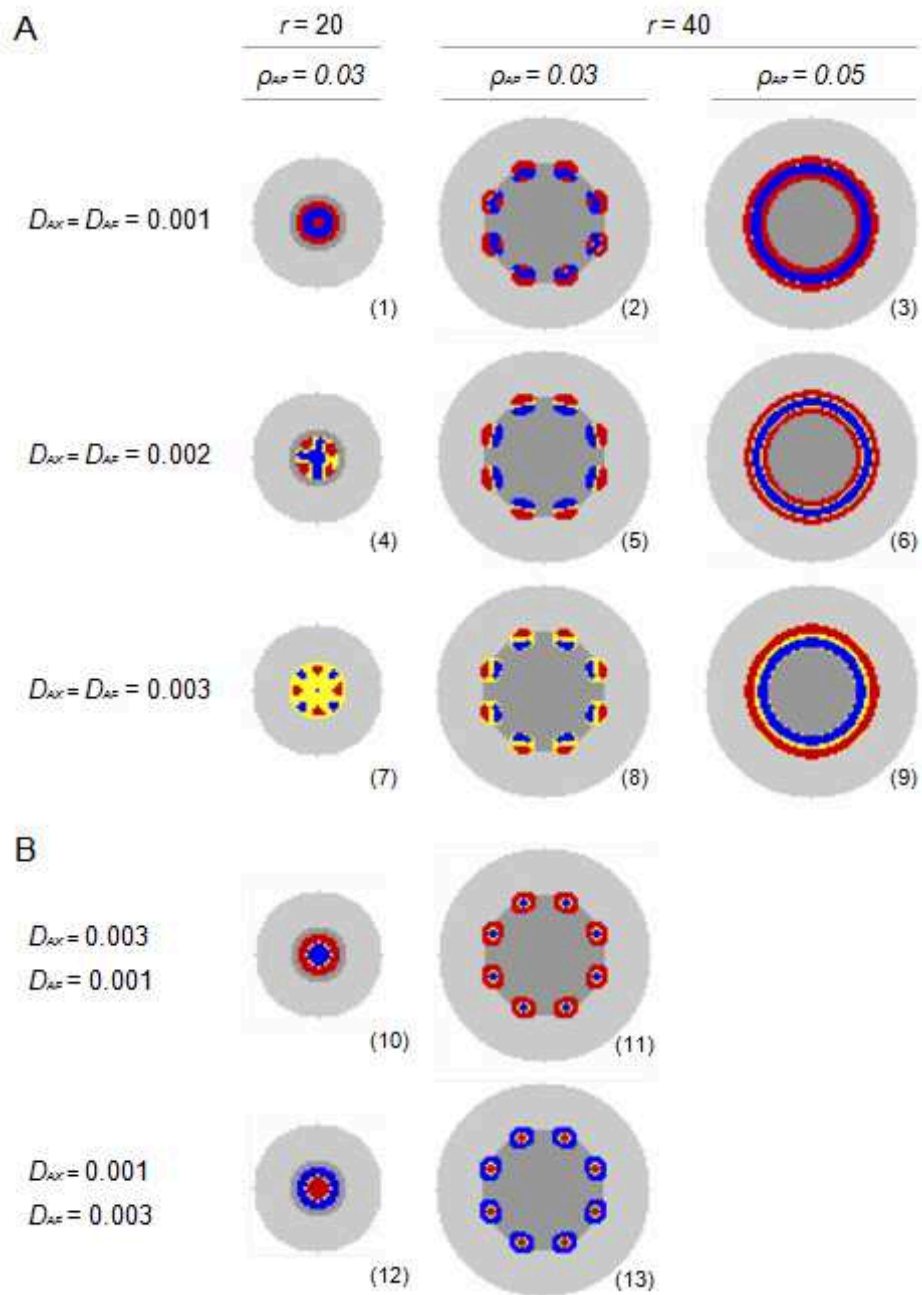
Figure 4.5. Effect of diffusion coefficients D_{AX} and D_{AF} and procambium configuration on xylem and phloem differentiation patterns. Other parameter values are listed in Tables 4.1 and 4.2. See text for details.

51

DISCUSSION

Since the beginning of the twentieth century, an increasing attention to the anatomical structure of vascular tissues in plants from evolutionary and developmental points of view is found in the botanical literature (e.g. Worsdell 1902; Jeffrey 1903). In the following decades, the focus shifted from macro and microscopic studies of anatomical features, to the investigation of genetic and physiological aspects of vascular differentiation (Sieburth and Deyholos 2006).

A great number of experimental studies, mainly on model plants like *Arabidopsis*, *Zinnia* and *Populus*, reported on plant hormones control of vascular development. Auxin, in particular, has been considered for its wide influence on several aspects of development, e.g. promoting cell division (Schrader *et al*. 2004), inducing the differentiation of xylem tracheary elements (Yoshida *et al*. 2009), formation and maintenance of vascular continuity along plant organs through its polar transport (Scarpella *et al*. 2006). Brassinosteroid was also found to play a role in promotion of cell expansion and vascular development (Vert and Chory 2006). Cytokinin was found to negatively regulate protoxylem specification in *Arabidopsis* (Mähönen *et al*. 2006). Many transcriptional regulators implicated in vascular cell specification have been recently identified. For example, MP is an auxin-responsive transcriptional activator, belonging to the family of ARFs, that regulates the specification of procambial cells *via* the induction of expression of *ATHB-8* (Donner *et al*. 2009).

Most experimental works focused on different specific aspects of the vascular development of plants, however, the interactions between the system components still need to be clarified in both their spatial and temporal processes. Recent modelling work by Muraro *et al*. (2013) showed the possibility to effectively simulate the molecular networks involved in xylem and procambium specification and their radial patterning. The authors developed a mathematical model incorporating auxin and cytokinin signalling networks and transport dynamics to test whether their mutually inhibitory interactions can explain vascular patterning. In particular, they were able to show that the restriction of *PHB* by miRNA165/166 is necessary for the establishment of the *Arabidopsis* root bisymmetric pattern and also that an unidentified component of the network is required to account for the spatial expression of *ARR5*.

The aim of our work was to investigate the spatial and temporal processes involved in vascular patterning that could also account for the diversity of steles observed in nature. Following this scope, we formulated a general modelling framework based on the reaction-diffusion systems proposed by Turing (1952) and applied by Meinhardt (1982) to animal and plant development.

The main feature of the proposed model is its ability to dynamically simulate developmental processes as different integrated modules. Moreover, the simplicity of the formulation allowed for the recognition of a limited number of parameters generating different emerging patterns of both procambium within the plant section, and phloem and xylem within each bundle. Simulation results showed that the model was capable of reproducing most vascular spatial patterns observed in plants, from primitive and simple structures, constituted of a single strand of vascular bundles (protostele), to more complex and evolved ones, with separated vascular bundles arranged in an ordered pattern within the plant section. An interesting result is the formation of the protostele for small simulation domains. This result seems to be consistent with the occurrence of this particular structure in species and organs with relatively smaller dimensions which are typically found in primitive plants (e.g. Pteridophyta). Noteworthy, apical meristems in roots are generally smaller than in shoots and the usual root vascular arrangement is the atactostele where peripheral spots of phloem are surrounded by internal xylem (Esau 1977). Figure 4.6 summarizes such results showing representative comparative examples between simulated patterns and transverse sections of different species.

All the reported patterns were determined under the assumption that phloem and xylem are specifically promoted in the peripheral and central zones respectively. As already mentioned, this assumption reflects the experimental evidences suggested by genetic analyses on *Arabidopsis* that genes involved in the specification of adaxial-abaxial (central-peripheral) polarity are also responsible for specification of phloem and xylem. We also investigated two different cases, i.e., the opposite facilitation condition (with phloem and xylem promoted in the central and peripheral zone respectively) and the case of complete absence of local facilitation. Interestingly, some spatial patterns resulted to be completely insensitive to facilitation, in particular the ones that emerged due to differences of the diffusion coefficients of the phloem and xylem activators (Fig. 4.5B). On the one hand, when opposed local facilitation was assumed, the radial patterns of phloem and xylem simply resulted to be inverted (data not shown). On the other hand, when no facilitation of the two activators was implemented ($\overline{\sigma_{SF}} = \overline{\sigma_{SX}} = 0$), the simulations generated an arrangement where phloem and xylem form alternated bands, a structure called plectostele (see Fig. 4.6) that is found, for instance, in plants of the genus *Lycopodium*.
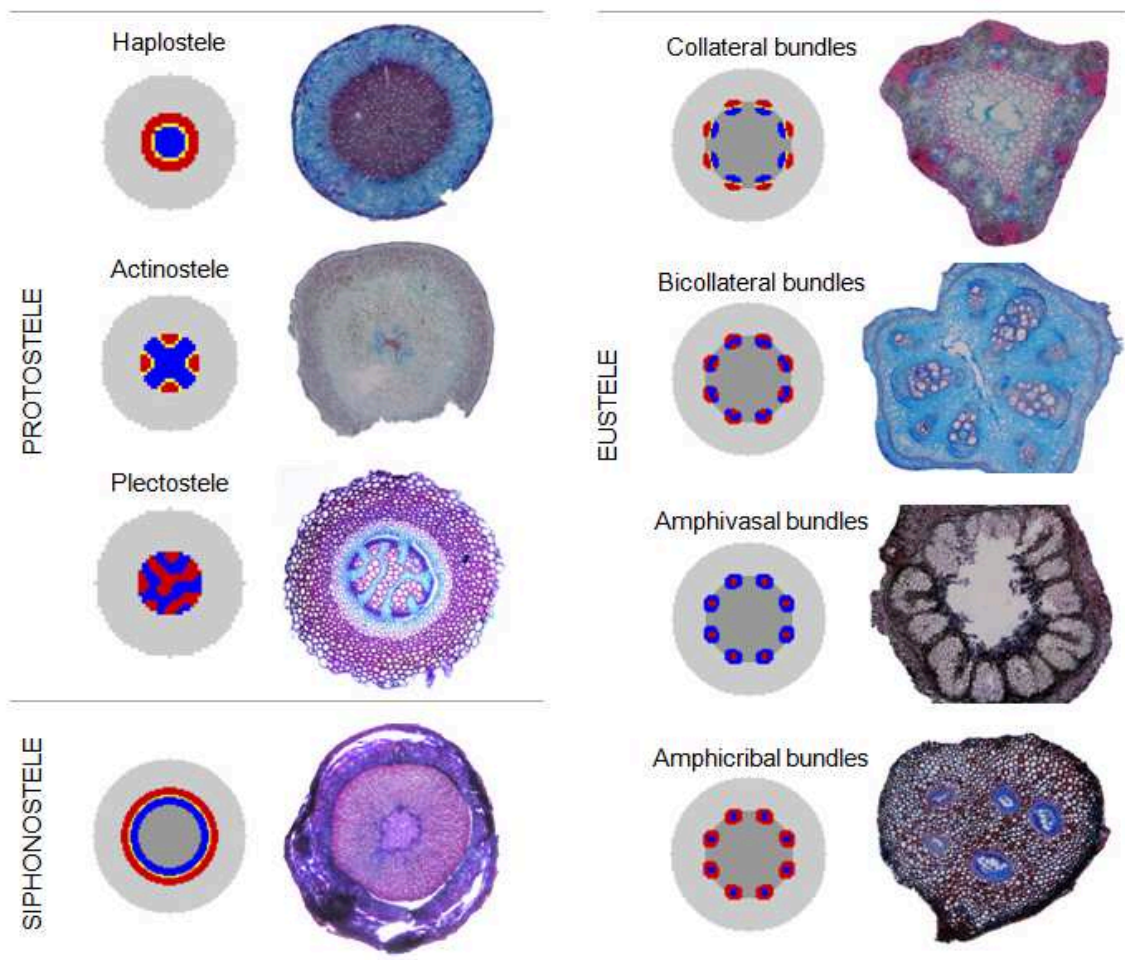
Figure 4.6. Spatial patterns of vascular tissues in both simulated and observed plant transverse sections. Haplostele: *Mespilus germanica* root. Actinostele: *Psilotum nudum* stem. Plectostele: *Lycopodium annotinum* stem. Siphonostele: *Mespilus germanica* stem. Eustele with collateral bundles: *Carex glareosa* stem. Eustele with bicollateral bundles: *Cucumis sativa* stem. Eustele with amphivasal bundles: *Osmunda regalis* stem. Eustele with amphicribal bundles: *Dryopteris robertiana* stem.

Another important structure, typical of the monocots, is the atactostele, generally defined as a "system of randomly scattered bundles", whereas it is clear that the system components have a specific and predictable behaviour (Beck *et al*. 1982). In monocotyledonous seedlings, the vascular system is arranged in a central cylinder very similar to that of dicotyledons (Tomlinson 1970). Afterwards, peripheral stem bundles originate from the disks of leaf insertion, where the midvein and secondary veins develop both acropetally through the leaf lamina and basipetally into the stem where they eventually connect with the stem vasculature (Nelson and Dengler 1997). For such reasons, the presented model is coherent with the development of vascular bundles also in monocots where the first and innermost set of bundles develops as a typical eustelic pattern and the formation of new leaves leads to the insertion of new veins within the stem, resulting in the final observed pattern (Fig. 4.7).

In conclusion, the model showed the capability of qualitatively reproduce the most diverse radial arrangements of vascular tissues. Future work could be done to perform a systematic comparison of our simulations with a more extensive set of observed patterns to verify, for instance, the prediction of structures not (yet) found in nature and to investigate the occurrence of the protostele in correlation to meristem size. Moreover, the model could be applied for comparative analysis with *Arabidopsis* mutants which show aberrant vascular patterns to better understand the relationships between specific gene functionality and anatomical development.
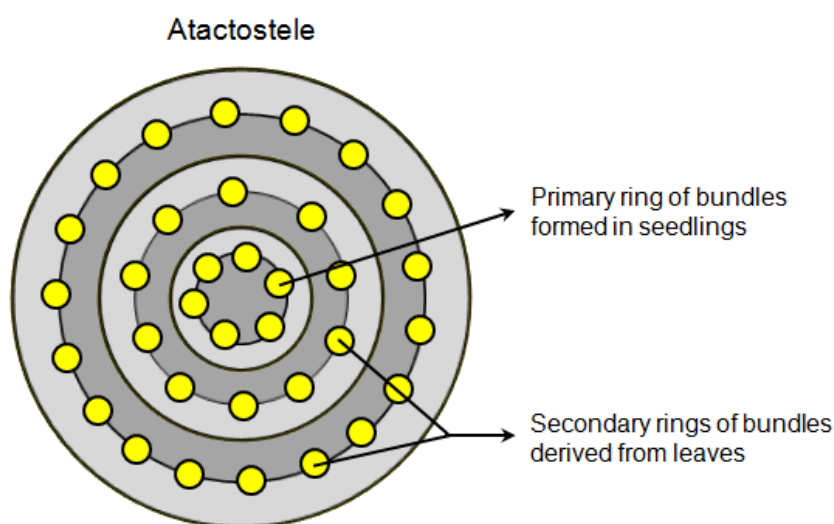
Figure 4.7. Schematic representation of the formation of the atactostele.

ACKNOWLEDGEMENTS

SUPPLEMENTARY INFORMATION

Supplementary videos (Video S1 and S2) can be found at the following web page:

http://wpage.unina.it/giannino/video/

5

CONCLUSIONS AND FUTURE PERSPECTIVES

The exponential evolution of technology and data collection techniques had an enormous impact on the recent history of scientific inquiry. While high resolution images and in-depth measurements highly increased the knowledge on specific processes, at the same time, this uncanny amount of available data diverted the attention of scientists from the global functioning of the systems they were studying.

Biological systems are very often complex and a reductionist approach is not the most appropriate to the study of complexity. This is also suggested by the etymology of the word complex itself. Complex is derived from the latin 'complexus' (past participle of the verb 'complecti') that means 'consisting of different and connected parts', this denotes a tight interrelation between the parts. As a matter of fact, a complex system is defined as a set of interacting components, whose relations are often non linear, presenting a global behaviour that is different from the behaviour of its single parts. From this definition it's easy to understand that an accurate study of the system components is useful and necessary, but is often not sufficient to understand the behaviour of the entire system. With these considerations in mind, this thesis presents a series of theoretical studies addressing two problems related to pattern formation in plants at different scales.

The role of self organization in vegetation pattern formation

The first study subject was the spontaneous formation of vegetation spatial patterns and the putative mechanisms responsible for their emergence. First, we reviewed the mechanistic explanations found in literature for this phenomenon (Chapters 2 and 3). The main body of work focuses the attention on the interactions between biomass and water, since such patterns are mainly observed in arid and semiarid environments. In order to explain the emergence of these patterns also in environments where water is not a limiting factor, we formulated a mathematical model to test the effects of the release of autotoxic compounds during litter decomposition, i.e. plant-soil negative feedback, on the emergence of vegetation patterns, in particular the formation of ring structures by clonal plants (Chapter 2). Simulation results show that autotoxicity can be a putative explanation for the formation of ring patterns during the colonization of bare substrates in primary successions. It is important to note a significant difference between water/biomass model outputs and the proposed biomass/toxicity model. The first formulation produces stable Turing patterns, while our formulation has only two equilibrium solutions, bare soil and uniform vegetation cover, meaning that the interactions between plant biomass and toxic compounds alone produce transient structures that, in time, always lead to homogeneous cover. This result is consistent with the fact that clear rings are not commonly observed in nature and frequently during new substrate colonization. This interesting result leads to new hypotheses on the formation and dynamics of rings by clonal plants that need to be experimentally verified. Moreover the research for the characterization of the compounds responsible for autotoxicity is ongoing using NMR-CPMAS methods. This new results should better clarify the importance of autotoxicity in the context of the plant-soil negative feedback and the ecological relevance of the phenomenon.

Furthermore, we also wanted to test the effects of both water and toxicity feedbacks on plant biomass dynamics and pattern formation (Chapter 3). Simulation results show that the effect of toxicity on the system is dependent on the decay rate of such compounds. For rapid removal rates of toxicity from soil, the effect is limited to a general reduction of the plants fitness. If the removal rate is lower, meaning a longer persistence of toxicity in soil, a surprising result appears, i.e. aggregated spots of plants are still formed due to the water/biomass feedbacks, but they constantly move in space to avoid the local accumulation of toxicity. Considering the slow growth rates of plants in arid environments, the described phenomenon is difficult to observe and further studies are highly recommended to test the model results. Moreover, simulations reveal that in case of toxic effects and moving plant spots, the biomass distribution along the spots should appear with a characteristic shape while other formulations predict a symmetrical distribution of biomass. This result has been preliminarily tested comparing simulations with satellite images and a more complete and robust analysis will be the subject of future studies.

The role of self organization in the development of plants

The second topic of this thesis was the differentiation of vascular tissues in plants and their spatial arrangements. In this part of the work (Chapter 4) we reviewed the current knowledge of the factors responsible for the specification of provascular tissues, phloem and xylem with a particular attention to the processes involved in their spatial positioning. Accordingly, we formulated a modular mathematical model that, starting from an homogeneous group of undifferentiated cells, reproduces the key developmental steps leading to the differentiation of primary vascular patterns. The results showed the capability of simulating both the position of vascular tissues along a radial section of stems and roots, and the arrangement of phloem and xylem within each bundle. Simulated structures were also qualitatively compared with patterns observed in nature. The numerical analysis of the model provided interesting insights related to the factors involved in the intra- and inter-specific variability of patterns. One example is the occurrence of protostelic structures for smaller simulation domains. Such structures are generally observed in roots and primitive plants. To test this prediction, a systematic analysis comparing the dimension of meristems of species and organs showing this particular arrangement will be performed in future studies. Moreover, in order to test the assumptions made during the formulation of the model, further work will be carried out to simulate aberrant patterns produced by mutations of key genes involved in vascular patterning of model species like *Arabidopsis*.

BIBLIOGRAPHY

Adachi N, Terashima I, Takahashi M. **1996**. Central die-back of monoclonal stands of Reynoutria japonica in an early stage of primary succession on Mount Fuji. *Annals of Botany* **77**: 477–486.

Armstrong J, Armstrong W. **2001**. An overview of the effects of phytotoxins on Phragmites australis in relation to die-back. *Aquatic Botany* **69**: 251–268.

Barbier N, Couteron P, Lefever R, Deblauwe V, Lejeune O. **2008**. Spatial decoupling of facilitation and competition at the origin of gapped vegetation patterns. *Ecology* **89**: 1521–31.

Bayer EM, Smith RS, Mandel T, Nakayama N, Sauer M, Prusinkiewicz P, Kuhlemeier C. **2009**. Integration of transport-based models for phyllotaxis and midvein formation. *Genes & Development* **23**: 373–84.

Beck CB, Schmid R, Rothwell GW. **1982**. Stelar morphology and the primary vascular system of seed plants. *The Botanical Review* **48**: 691–815.

Benítez M, Espinosa-Soto C, Padilla-Longoria P, Díaz J, Alvarez-Buylla ER. **2007**. Equivalent genetic regulatory networks in different contexts recover contrasting spatial cell patterns that resemble those in Arabidopsis root and leaf epidermis: a dynamic model. *The International Journal of Developmental Biology* **51**: 139–55.

Bever JD. **1994**. Feeback between plants and their soil communities in an old field community. *Ecology* **75**: 1965–1977.

Bever JD, Westover KM, Antonovics J. **1997**. Incorporating the soil community into plant population dynamics: the utility of the feedback approach. *Journal of Ecology* **85**: 561–573.

Bishopp A, Help H, El-Showk S, Weijers D, Scheres B, Friml J, Benková E, Mähönen AP, Helariutta Y. **2011**. A mutually inhibitory interaction between auxin and cytokinin specifies vascular pattern in roots. *Current Biology* **21**: 917–926.

Bishopp A, Lehesranta S, Vatén A, Help H, El-Showk S, Scheres B, Helariutta K, Mähönen AP, Sakakibara H, Helariutta Y. **2011**. Phloem-transported cytokinin regulates polar auxin transport and maintains vascular pattern in the root meristem. *Current Biology* **21**: 927–932.

Blilou I, Xu J, Wildwater M, Willemsen V, Paponov I, Friml J, Heidstra R, Aida M, Palme K, Scheres B. **2005**. The PIN auxin efflux facilitator network controls growth and patterning in Arabidopsis roots. *Nature* **433**: 39–44.

Blok WJ, Bollen GJ. **1993**. The role of autotoxins from root residues of the previous crop in the replant disease of asparagus. *Netherlands Journal of Plant Pathology* **99**: 29–40.

Blomqvist MM, Olff H, Blaauw MB, Bongers T, van der Putten WH. **2000**. Interactions between above- and belowground biota: importance for small-scale vegetation mosaics in a grassland ecosystem. *Oikos* **90**: 582–598.

Boaler SB, Hodge CAH. **1964**. Observations on vegetation arcs in the northern region, Somali Republic. *Journal of Ecology* **52**: 511–544.

Bonanomi G. **2002**. *Il ruolo dell'eterogeneità ambientale, indotta dalla piñata mediante il rinnovo aereo e radicale, sulla biodiversità a scala di comunità*. PhD Thesis, University of Ancona, Italy.

Bonanomi G, Allegrezza M. **2004**. Effetti della colonizzazione di Brachypodium rupestre (Host) Roemer et Schultes sulla diversità fitocenotica in un settore dell'Appennino umbro-marchigiano. *Fitosociologia* **41**: 51–69.

Bonanomi G, Antignani V, Barile E, Lanzotti V, Scala F. **2011**. Decomposition of Medicago sativa residues affects phytotoxicity, fungal growth and soil-borne pathogen diseases. *Journal of Plant Pathology* **93**: 57–69.

Bonanomi G, Antignani V, Capodilupo M, Scala F. **2010**. Identifying the characteristics of organic soil amendments that suppress soilborne plant diseases. *Soil Biology and Biochemistry* **42**: 136–144.

Bonanomi G, Antignani V, Pane C, Scala F. **2007**. Suppression of soilborne fungal diseases with organic amendments. *Journal of Plant Pathology* **89**: 311–324.

Bonanomi G, Giannino F, Mazzoleni S. **2005**. Negative plant-soil feedback and species coexistence. *Oikos* **111**: 311–321.

Bonanomi G, Incerti G, Allegrezza M. **2013**. Assessing the impact of land abandonment, nitrogen enrichment and fairy-ring fungi on plant diversity of Mediterranean grasslands. *Biodiversity and Conservation* **22**: 2285–2304.

Bonanomi G, Incerti G, Barile E, Capodilupo M, Antignani V, Mingo A, Lanzotti V, Scala F, Mazzoleni S. **2011**. Phytotoxicity, not nitrogen immobilization, explains plant litter inhibitory effects: evidence from solid-state 13C NMR spectroscopy. *New Phytologist* **191**: 1018–30.

Bonanomi G, Mingo A, Incerti G, Mazzoleni S, Allegrezza M. **2012**. Fairy rings caused by a killer fungus foster plant diversity in species-rich grassland (M Zobel, Ed.). *Journal of Vegetation Science* **23**: 236–248.

Bonanomi G, Rietkerk M, Dekker SC, Mazzoleni S. **2005**. Negative plant–soil feedback and positive species interaction in a herbaceous plant community. *Plant Ecology* **181**: 269–278.

Bonanomi G, Rietkerk M, Dekker SC, Mazzoleni S. **2007**. Islands of fertility induce co-occurring negative and positive plant-soil feedbacks promoting coexistence. *Plant Ecology* **197**: 207–218.

Bonanomi G, Sicurezza MG, Caporaso S, Esposito A, Mazzoleni S. **2006**. Phytotoxicity dynamics of decaying plant materials. *New Phytologist* **169**: 571–8.

Bonke M, Thitamadee S, Mähönen AP, Hauser M-T, Helariutta Y. **2003**. APL regulates vascular tissue identity in Arabidopsis. *Nature* **426**: 181–186.

Bowman JL, Floyd SK. **2008**. Patterning and polarity in seed plant shoots. *Annual Review of Plant Biology* **59**: 67–88.

Caldwell P-A. **1957**. The spatial development of Spartina colonies growing without competition. *Annals of Botany* **21**: 203–214.

Camazine S, Deneubourg J-L, Franks N, Sneyd J, Theraulaz G, Bonabeau E. **2001**. *Self-organization in biological systems*. Princeton, NJ.: Princeton University Press.

Caño-Delgado A, Lee J-Y, Demura T. **2010**. Regulatory mechanisms for specification and patterning of plant vascular tissues. *Annual Review of Cell and Developmental Biology* **26**: 605–637.

Carlsbecker A, Helariutta Y. **2005**. Phloem and xylem specification: pieces of the puzzle emerge. *Current Opinion in Plant Biology* **8**: 512–517.

Carteni F, Marasco A, Bonanomi G, Mazzoleni S, Rietkerk M, Giannino F. **2012**. Negative plant soil feedback explaining ring formation in clonal plants. *Journal of Theoretical Biology* **313**: 153–161.

Castellanos EM, Figueroa ME, Davy AJ. **1994**. Nucleation and facilitation in saltmarsh succession: interactions between Spartina maritima and Arthrocnemum perenne. *Journal of Ecology* **82**: 239–248.

Castets V, Dulos E, Boissonade J, De Kepper P. **1990**. Experimental evidence of a sustained standing Turing-type nonequilibrium chemical pattern. *Physical Review Letters* **64**: 2953–2956.

Cosby HE. **1960**. Rings on the range. *Journal of Range Management Archives* **13**: 283–288.

Coullet P, Riera C, Tresser C. **2000**. Stable static localized structures in one dimension. *Physical Review Letters* **84**: 3069–72.

Curtis JT, Cottam G. **1950**. Antibiotic and autotoxic effects in prairie sunflower. *Bulletin of the Torrey Botanical Club* **77**: 187–191.

Danin A. **1996**. *Plants of Desert Dunes*. Berlin: Springer.

Deblauwe V, Barbier N, Couteron P, Lejeune O, Bogaert J. **2008**. The global biogeography of semi-arid periodic vegetation patterns. *Global Ecology and Biogeography* **17**: 715–723.

Dekker SC, de Boer HJ, Brovkin V, Fraedrich K, Wassen MJ, Rietkerk M. **2010**. Biogeophysical feedbacks trigger shifts in the modelled vegetation-atmosphere system at multiple scales. *Biogeosciences* **7**: 1237–1245.

Digiuni S, Schellmann S, Geier F, Greese B, Pesch M, Wester K, Dartan B, Mach V, Srinivas BP, Timmer J, Fleck C, Hulskamp M. **2008**. A competitive complex formation mechanism underlies trichome patterning on Arabidopsis leaves. *Molecular Systems Biology* **4**: 1–11.

Donner TJ, Sherr I, Scarpella E. **2009**. Regulation of preprocambial cell state acquisition by auxin signaling in Arabidopsis leaves. *Development* **136**: 3235–3246.

Doust LL. **1981**. Population dynamics and local specialization in a clonal perennial (Ranunculus repens): I. The dynamics of ramets in contrasting habitats. *Journal of Ecology* **69**: 743–755.

Dowson C, Rayner A, Boddy L. **1989**. Spatial dynamics and interactions of the woodland fairy ring fungus, Clitocybe nebularis. *New Phytologist* **111**: 699–705.

Ehrenfeld JG, Ravit B, Elgersma K. **2005**. Feedback in the plant-soil system. *Annual Review of Environment and Resources* **30**: 75–115.

Emery JF, Floyd SK, Alvarez J, Eshed Y, Hawker NP, Izhaki A, Baum SF, Bowman JL. **2003**. Radial patterning of Arabidopsis shoots by class III HD-ZIP and KANADI genes. *Current Biology* **13**: 1768–1774.

Eppinga MB, Rietkerk M, Borren W, Lapshina ED, Bleuten W, Wassen MJ. **2008**. Regular surface patterning of peatlands: confronting theory with field data. *Ecosystems* **11**: 520–536.

Eppinga MB, de Ruiter PC, Wassen MJ, Rietkerk M. **2009**. Nutrients and hydrology indicate the driving mechanisms of peatland surface patterning. *The American Naturalist* **173**: 803–18.

Esau K. **1977**. *Anatomy of Seed Plants*. New York: Wiley.

Eshed Y, Baum SF, Perea J V., Bowman JL. **2001**. Establishment of polarity in lateral organs of plants. *Current Biology* **11**: 1251–1260.

Eveland AL, Jackson DP. **2011**. Sugars, signalling, and plant development. *Journal of Experimental Botany* **63**: 3367–3377.

Falinska K. **1995**. Genet disintegration in Filipendula ulmaria: consequences for population dynamics and vegetation succession. *Journal of Ecology* **83**: 9–21.

Feugier FG, Mochizuki A, Iwasa Y. **2005**. Self-organization of the vascular system in plant leaves: inter-dependent dynamics of auxin flux and carrier proteins. *Journal of Theoretical Biology* **236**: 366–75.

Fisher RA. **1937**. The wave of advance of advantageous genes. *Annals of Eugenics* **7**: 355–369.

Flach EH, Schnell S. **2006**. Use and abuse of the quasi-steady-state approximation. *Systems Biology* **153**: 187–91.

Fujita H, Toyokura K, Okada K, Kawaguchi M. **2011**. Reaction-diffusion pattern in shoot apical meristem of plants. *PLoS ONE* **6**: e18243.

Gilad E, von Hardenberg J, Provenzale A, Shachak M, Meron E. **2007**. A mathematical model of plants as ecosystem engineers. *Journal of Theoretical Biology* **244**: 680–91.

Grieneisen V a, Xu J, Marée AFM, Hogeweg P, Scheres B. **2007**. Auxin transport is sufficient to generate a maximum and gradient guiding root growth. *Nature* **449**: 1008–13.

Haken H. **2006**. *Information and self-organization: a macroscopic approach to complex systems*. Berlin: Springer.

Von Hardenberg J, Kletter AY, Yizhaq H, Nathan J, Meron E. **2010**. Periodic versus scale-free patterns in dryland vegetation. *Proceedings of the Royal Society of London. Series B, Biological Sciences* **277**: 1771–6.

Von Hardenberg J, Meron E, Shachak M, Zarmi Y. **2001**. Diversity of vegetation patterns and desertification. *Physical Review Letters* **87**: 198101.

Hardtke CS, Berleth T. **1998**. The Arabidopsis gene MONOPTEROS encodes a transcription factor mediating embryo axis formation and vascular development. *The EMBO Journal* **17**: 1405–11.

Heslop-Harrison Y, Heslop-Harrison J. **1958**. Ring formation by Triglochin maritima in Eastern Irish Salt Marsh. *The Irish Naturalists' Journal* **12**: 223–229.

HillerisLambers R, Rietkerk MG, van den Bosch F, Prins HHT, Kroon H de. **2001**. Vegetation pattern formation in semi-arid grazing systems. *Ecology* **82**: 50–61.

Hitchcock AS. **1935**. *Manual of the grasses of the United States*. United States Government Printing Office, Washington.

Hoitink H, Boehm M. **1999**. Biocontrol within the context of soil microbial communities: a substrate-dependent phenomenon. *Annual Review of Phytopathology* **37**: 427–446.

Holmes EE, Lewis MA, Banks JE, Veit RR. **1994**. Partial differential equations in ecology: spatial interactions and population dynamics. *Ecology* **75**: 17–29.

Ilegems M, Douet V, Meylan-Bettex M, Uyttewaal M, Brand L, Bowman JL, Stieger PA. **2010**. Interplay of auxin, KANADI and Class III HD-ZIP transcription factors in vascular tissue formation. *Development* **137**: 975–984.

Jeffrey EC. **1903**. The structure and development of the stem in the Pteridophyta and gymnosperms. *Philosophical Transactions of the Royal Society of London. Series B, Containing Papers of a Biological Character* **195**: 119–146.

Jensen O, Pannbacker V, Mosekilde E, Dewel G, Borckmans P. **1994**. Localized structures and front propagation in the Lengyel-Epstein model. *Physical Review E* **50**: 736–749.

Jönsson H, Gruel J, Krupinski P, Troein C. **2012**. On evaluating models in Computational Morphodynamics. *Current Opinion in Plant Biology* **15**: 103–110.

Jönsson H, Heisler M, Reddy GV, Agrawal V, Gor V, Shapiro BE, Mjolsness E, Meyerowitz EM. **2005**. Modeling the organization of the WUSCHEL expression domain in the shoot apical meristem. *Bioinformatics* **21**: i232–40.

Jönsson H, Krupinski P. **2010**. Modeling plant growth and pattern formation. *Current Opinion in Plant Biology* **13**: 5–11.

Jönsson H, Shapiro BE, Meyerowitz EM, Mjolsness E. **2003**. Signalling in multicellular models of plant development. *On Growth, Form, and Computers*. London: Academic Press, .

Kardol P, Cornips NJ, van Kempen MML, Bakx-Schotman JMT, van der Putten WH. **2007**. Microbe-mediated plant-soil feedback causes historical contingency effects in plant community assembly. *Ecological Monographs* **77**: 147–162.

Kéfi S, Eppinga MB, Ruiter PC, Rietkerk M. **2010**. Bistability and regular spatial patterns in arid ecosystems. *Theoretical Ecology* **3**: 257–269.

Kerstetter RA, Bollman K, Taylor RA, Bomblies K, Poethig RS. **2001**. KANADI regulates organ polarity in Arabidopsis. *Nature* **411**: 706–9.

Kessler MA, Werner BT. **2003**. Self-organization of sorted patterned ground. *Science* **299**: 380–3.

Klausmeier CA. **1999**. Regular and irregular patterns in semiarid vegetation. *Science* **284**: 1826–1828.

Klironomos JN. **2002**. Feedback with soil biota contributes to plant rarity and invasiveness in communities. *Nature* **417**: 67–70.

Kolmogorov AN, Petrovsky IG, Piskunov NS. **1937**. Investigation of the equation of diffusion combined with increasing of the substance and its application to a biology problem. *Bull. Moscow State Univ. Ser. A: Math. Mech.* **6**: 1–25.

Kondo S, Miura T. **2010**. Reaction-diffusion model as a framework for understanding biological pattern formation. *Science* **329**: 1616–20.

Van de Koppel J, Rietkerk MG, Dankers N, Herman PMJ. **2005**. Scale-dependent feedback and regular spatial patterns in young mussel beds. *The American Naturalist* **165**: E66–E77.

Van de Koppel J, Rietkerk M, Weissing FJ. **1997**. Catastrophic vegetation shifts and soil degradation in terrestrial grazing systems. *Trends in Ecology & Evolution* **12**: 352–356.

Kulmatiski A, Beard KH, Stevens JR, Cobbold SM. **2008**. Plant-soil feedbacks: a meta-analytical review. *Ecology letters* **11**: 980–92.

Lanta V, Dolezal J, Samata J. **2004**. Vegetation patterns in a cut-away peatland in relation to abiotic and biotic factors : a case study from the Šumava Mts ., Czech Republic. *Suo* **55**: 33–43.

Lanta V, Janeček Š, Doležal J. **2008**. Radial growth and ring formation process in clonal plant Eriophorum angustifolium on post-mined peatland in the Šumava Mts., Czech Republic. *Annales Botanici Fennici* **45**: 44–54.

Lefever R, Lejeune O. **1997**. On the origin of tiger bush. *Bulletin of Mathematical Biology* **59**: 263–294.

Lejeune O, Couteron P, Lefever R. **1999**. Short range co-operativity competing with long range inhibition explains vegetation patterns. *Acta Oecologica* **20**: 171–183.

Lejeune O, Tlidi M, Couteron P. **2002**. Localized vegetation patches: a self-organized response to resource scarcity. *Physical Review. E, Statistical, Nonlinear, and Soft Matter Physics* **66**: 010901.

Leprun JC. **1999**. The influences of ecological factors on tiger bush and dotted bush patterns along a gradient from Mali to northern Burkina Faso. *Catena* **37**: 25–44.

Lewis JP, Stofella SL, Feldman SR. **2001**. Monk's tonsure-like gaps in the tussock grass Spartina argentinensis (Gramineae). *Revista de Biología Tropical* **49**: 313–316.

Mähönen AP, Bishopp A, Higuchi M, Nieminen KM, Kinoshita K, Törmäkangas K, Ikeda Y, Oka A, Kakimoto T, Helariutta Y. **2006**. Cytokinin signaling and its inhibitor AHP6 regulate cell fate during vascular development. *Science* **311**: 94–8.

Marasco A, Iuorio A, Carteni F, Bonanomi G, Giannino F, Mazzoleni S. **2013**. Water limitation and negative plant-soil feedback explain vegetation patterns along rainfall gradient. *Procedia Environmental Sciences* **19**: 139–147.

Mazzoleni S, Bonanomi G, Giannino F, Incerti G, Dekker SC, Rietkerk M. **2010**. Modelling the effects of litter decomposition on tree diversity patterns. *Ecological Modelling* **221**: 2784–2792.

Mazzoleni S, Bonanomi G, Giannino F, Rietkerk MG, Dekker SC, Zucconi F. **2007**. Is plant biodiversity driven by decomposition processes? An emerging new theory on plant diversity. *Community Ecology* **8**: 103–109.

Meinhardt H. **1982**. *Models of biological pattern formation*. London: Academic Press.

Meinhardt H. **1995**. *The algorithmic beauty of sea shells*. Berlin: Springer.

Meinhardt H, Gierer A. **1980**. Generation and regeneration of sequence of structures during morphogenesis. *Journal of Theoretical Biology* **85**: 429–450.

Meron E. **2010**. Modeling dryland landscapes. *Mathematical Modelling of Natural Phenomena* **6**: 163–187.

Meron E, Gilad E, von Hardenberg J, Shachak M, Zarmi Y. **2004**. Vegetation patterns along a rainfall gradient. *Chaos, Solitons & Fractals* **19**: 367–376.

Meron E, Yizhaq H, Gilad E. **2007**. Localized structures in dryland vegetation: forms and functions. *Chaos* **17**: 037109.

Mitchison GJ. **1980**. A model for vein formation in higher plants. *Proceedings of the Royal Society of London. Series B, Biological Sciences* **207**: 79–109.

Muraro D, Mellor N, Pound MP, Help H, Lucas M, Chopard J, Byrne HM, Godin C, Hodgman TC, King JR, Pridmore TP, Helariutta Y, Bennett MJ, Bishopp A. **2013**. Integration of hormonal signaling networks and mobile microRNAs is required for vascular patterning in Arabidopsis roots. *Proceedings of the National Academy of Sciences of the United States of America* **111**: 857–862.

Murray JD. **2002**. *Mathematical Biology : I . An Introduction, Third Edition*. New York: Springer.

Nathan J, von Hardenberg J, Meron E. **2013**. Spatial instabilities untie the exclusion-principle constraint on species coexistence. *Journal of Theoretical Biology* **335**: 198–204.

Nelson T, Dengler N. **1997**. Leaf Vascular Pattern Formation. *The Plant Cell* **9**: 1121–1135.

Okayasu T, Aizawa Y. **2001**. Systematic analysis of periodic vegetation patterns. *Progress of Theoretical Physics* **106**: 705–720.

Olff H, Hoorens B, de Goede RGM, van der Putten WH, Gleichman JM. **2000**. Small-scale shifting mosaics of two dominant grassland species: the possible role of soil-borne pathogens. *Oecologia* **125**: 45–54.

Oremus PAI, Otten H. **1981**. Factors affecting growth and nodulation of Hippophaë rhamnoides L. ssp. Rhamnoides in soils from two successional stages of dune formation. *Plant and Soil* **63**: 317–331.

Otfinowski R. **2008**. *Patterns and processes of exotic plant invasions in Riding Mountain National Park, Manitoba, Canada*. Ph.D. Thesis.

Ouyang Q, Swinney HL. **1991**. Transition from a uniform state to hexagonal and striped Turing patterns. *Nature* **352**: 610–612.

Packer A, Clay K. **2000**. Soil pathogens and spatial patterns of seedling mortality in a temperate tree. *Nature* **404**: 278–81.

Patrick ZA, Toussoun TA. **1965**. Plant residues and organic amendments in relation to biological control. In: Baker FK, Snyder WC, eds. *Ecology of Soil-Borne Pathogens - Prelude to Biological Control*. University of California, Berkeley, CA, USA, 440–459.

Pemadasa MA. **1981**. Cyclic change and pattern in an Arthrocnemum community in Sri Lanka. *Journal of Ecology* **69**: 565–574.

Perry LG, Thelen GC, Ridenour WM, Weir TL, Callaway RM, Paschke MW, M. Vivanco J. **2005**. Dual role for an allelochemical: (±)-catechin from Centaurea maculosa root exudates regulates conspecific seedling establishment. *Journal of Ecology* **93**: 1126–1135.

Pesch M, Hülskamp M. **2004**. Creating a two-dimensional pattern de novo during Arabidopsis trichome and root hair initiation. *Current Opinion in Genetics and Development* **14**: 422–7.

Petrovskii S, Kawasaki K, Takasu F, Shigesada N. **2001**. Diffusive waves, dynamical stabilization and spatio-temporal chaos in a community of three competitive species. *Japan Journal of Industrial and Applied Mathematics* **18**: 459–481.

Pien S, Wyrzykowska J, Fleming AJ. **2001**. Novel marker genes for early leaf development indicate spatial regulation of carbohydrate metabolism within the apical meristem. *The Plant Journal* **25**: 663–674.

Pignatti S. **1997**. *Ecologia del paesaggio*. Torino: UTET.

Prusinkiewicz P, Runions A. **2012**. Computational models of plant development and form. *New Phytologist* **193**: 549–69.

Van der Putten WH. **2003**. Plant defense belowground and spatiotemporal processes in natural vegetation. *Ecology* **84**: 2269–2280.

Van der Putten WH, van Dijk C, Peters BAM. **1993**. Plant-specific soil-borne diseases contribute to succession in foredune vegetation. *Nature* **362**: 53–56.

Ravi S, D'Odorico P, Wang L, Collins S. **2008**. Form and function of grass ring patterns in arid grasslands: the role of abiotic controls. *Oecologia* **158**: 545–55.

Rietkerk MG, Boerlijst M, Langevelde F van, HillerisLambers R, Koppel J van de, Kumar L, Prins HHT, Roos AM de. **2002**. Self-organization of vegetation in arid ecosystems. *The American Naturalist* **160**: 524–530.

Rietkerk MG, van den Bosch F, van de Koppel J. **1997**. Site-specific properties and irreversible vegetation changes in semi-arid grazing systems. *Oikos* **80**: 241–252.

Rietkerk M, Dekker SC, de Ruiter PC, van de Koppel J. **2004**. Self-organized patchiness and catastrophic shifts in ecosystems. *Science* **305**: 1926–9.

Rietkerk M, van de Koppel J. **2008**. Regular pattern formation in real ecosystems. *Trends in Ecology & Evolution* **23**: 169–75.

Rovinsky AB, Menzinger M. **1993**. Self-organization induced by the differential flow of activator and inhibitor. *Physical Review Letters* **70**: 778–781.

Sachs T. **1969**. Polarity and the induction of organized vascular tissues. *Annals of Botany* **33**: 263–275.

Savage N Saint, Walker T, Wieckowski Y, Schiefelbein J, Dolan L, Monk N a M. **2008**. A mutual support mechanism through intercellular movement of CAPRICE and GLABRA3 can pattern the Arabidopsis root epidermis. *PLoS Biology* **6**: e235.

Scarpella E, Marcos D, Friml J, Berleth T. **2006**. Control of leaf vascular patterning by polar auxin transport. *Genes & Development* **20**: 1015–27.

Scheffer M, Bascompte J, Brock WA, Brovkin V, Carpenter SR, Dakos V, Held H, van Nes EH, Rietkerk M, Sugihara G. **2009**. Early-warning signals for critical transitions. *Nature* **461**: 53–9.

Schrader J, Nilsson J, Mellerowicz E, Berglund A, Nilsson P, Hertzberg M, Sandberg G. **2004**. A high-resolution transcript profile across the wood-forming meristem of poplar identifies potential regulators of cambial stem cell identity. *The Plant Cell* **16**: 2278–92.

Sheffer E, Yizhaq H, Gilad E, Shachak M, Meron E. **2007**. Why do plants in resource-deprived environments form rings? *Ecological Complexity* **4**: 192–200.

Sheffer E, Yizhaq H, Shachak M, Meron E. **2011**. Mechanisms of vegetation-ring formation in water-limited systems. *Journal of Theoretical Biology* **273**: 138–46.

Sherratt JA. **2005**. An analysis of vegetation stripe formation in semi-arid landscapes. *Journal of Mathematical Biology* **51**: 183–97.

Sherratt JA. **2010**. Pattern solutions of the Klausmeier model for banded vegetation in semi-arid environments I. *Nonlinearity* **23**: 2657–2675.

Sherratt JA, Lord GJ. **2007**. Nonlinear dynamics and pattern bifurcations in a model for vegetation stripes in semi-arid environments. *Theoretical Population Bology* **71**: 1–11.

Sieburth LE, Deyholos MK. **2006**. Vascular development: the long and winding road. *Current Opinion in Plant Biology* **9**: 48–54.

Singh HP, Batish DR, Kohli RK. **1999**. Autotoxicity: concept, organisms, and ecological significance. *Critical Reviews in Plant Sciences* **18**: 757–772.

Teale WD, Paponov I a, Palme K. **2006**. Auxin in action: signalling, transport and the control of plant growth and development. *Nature Reviews Molecular Cell Biology* **7**: 847–59.

Tlidi M, Mandel P, Lefever R. **1994**. Localized structures and localized patterns in optical bistability. *Physical Review Letters* **73**: 640–643.

Tomlinson PB. **1970**. Monocotyledons - towards an understanding of their morphology and anatomy. *Advances in Botanical Research* **3**: 207–292.

Turing AM. **1952**. The chemical basis of morphogenesis. *Philosophical Transactions of the Royal Society B: Biological Sciences* **237**: 37–72.

Ursino N, Contarini S. **2006**. Stability of banded vegetation patterns under seasonal rainfall and limited soil moisture storage capacity. *Advances in Water Resources* **29**: 1556–1564.

Valentin C, D'Herbès J., Poesen J. **1999**. Soil and water components of banded vegetation patterns. *Catena* **37**: 1–24.

Vanstraelen M, Benková E. **2012**. Hormonal interactions in the regulation of plant development. *Annual Review of Cell and Developmental Biology* **28**: 463–87.

Vert G, Chory J. **2006**. Downstream nuclear events in brassinosteroid signalling. *Nature* **441**: 96–100.

Volpert V, Petrovskii S. **2009**. Reaction-diffusion waves in biology. *Physics of Life Reviews* **6**: 267–310.

Waites R, Selvadurai HRN, Oliver IR, Hudson A. **1998**. The PHANTASTICA Gene Encodes a MYB Transcription Factor Involved in Growth and Dorsoventrality of Lateral Organs in Antirrhinum. *Cell* **93**: 779–789.

Watt AS. **1947**. Pattern and process in the plant community. *Journal of Ecology* **35**: 1–22.

Webb L, Tracey J, Haydock K. **1967**. A factor toxic to seedlings of the same species associated with living roots of the non-gregarious subtropical rain forest tree Grevillea robusta. *Journal of Applied Ecology* **4**: 13–25.

White LP. **1971**. Vegetation stripes on sheet wash surfaces. *Journal of Ecology* **59**: 615–622.

Wickens GE, Collier FW. **1971**. Some vegetation patterns in the Republic of the Sudan. *Geoderma* **6**: 43–59.

Wilson JW. **1978**. The position of regenerating cambia: auxin/sucrose ratio and the gradient induction hypothesis. *Proceedings of the Royal Society of London. Series B, Biological Sciences* **203**: 153–176.

Wolters H, Jürgens G. **2009**. Survival of the flexible: hormonal growth control and adaptation in plant development. *Nature Reviews Genetics* **10**: 305–17.

Worsdell WC. **1902**. The evolution of the vascular tissue of plants. *Botanical Gazette* **34**: 216–223.

Yoshida S, Iwamoto K, Demura T, Fukuda H. **2009**. Comprehensive analysis of the regulatory roles of auxin in early transdifferentiation into xylem cells. *Plant molecular biology* **70**: 457–69.

Zelnik YR, Kinast S, Yizhaq H, Bel G, Meron E. **2013**. Regime shifts in models of dryland vegetation. *Philosophical Transactions. Series A, Mathematical, Physical, and Engineering Sciences* **371**: 20120358.